Cellular/Molecular

Pharmacological Signature and Target Specificity of Inhibitory Circuits Formed by Martinotti Cells in the Mouse Barrel Cortex

Cristina Donato, Daniella Balduino Victorino, Carolina Cabezas, Andrea Aguirre, Joana Lourenço, Marie-Claude Potier, Javier Zorrilla de San Martin, and Alberto Bacci

Sorbonne Université; ICM - Institut du Cerveau, Paris Brain Institute; Centre National de la Recherche Scientifique (CNRS); Institut National de la Santé et de la Recherche Médicale (INSERM); Hôpital de la Pitié-Salpêtrière, 75013 Paris, France

In the neocortex, fast synaptic inhibition orchestrates both spontaneous and sensory-evoked activity. GABAergic interneurons (INs) inhibit pyramidal neurons (PNs) directly, modulating their output activity and thus contributing to balance cortical networks. Moreover, several IN subtypes also inhibit other INs, forming specific disinhibitory circuits, which play crucial roles in several cognitive functions. Here, we studied a subpopulation of somatostatin-positive INs, the Martinotti cells (MCs) in layer 2/3 of the mouse barrel cortex (both sexes). MCs inhibit the distal portion of PN apical dendrites, thus controlling dendrite electrogenesis and synaptic integration. Yet, it is poorly understood whether MCs inhibit other elements of the cortical circuits, and the connectivity properties with non-PN targets are unknown. We found that MCs have a strong preference for PN dendrites, but they also considerably connect with parvalbumin-positive, vasoactive intestinal peptide-expressing, and layer 1 (L1) INs. Remarkably, GABAergic synapses from MCs exhibited clear cell type-specific short-term plasticity. Moreover, whereas the biophysical properties of MC-PN synapses were consistent with distal dendritic inhibition, MC-IN synapses exhibited characteristics of fast perisomatic inhibition. Finally, MC-PN connections used α5-containing GABA$_A$ receptors (GABA$_A$Rs), but this subunit was not expressed by the other INs targeted by MCs. We reveal a specialized connectivity blueprint of MCs within different elements of superficial cortical layers. In addition, our results identify α5-GABA$_A$Rs as the molecular fingerprint of MC-PN dendritic inhibition. This is of critical importance, given the role of α5-GABA$_A$Rs in cognitive performance and their involvement in several brain diseases.

Key words: GABA alpha5; inhibitory synapses; interneurons; Martinotti cells; neocortex; somatostatin

Significance Statement

Martinotti cells (MCs) are a prominent, broad subclass of somatostatin-expressing GABAergic interneurons, specialized in controlling distal dendrites of pyramidal neurons (PNs) and taking part in several cognitive functions. Here we characterize the connectivity pattern of MCs with other interneurons in the superficial layers (L1 and L2/3) of the mouse barrel cortex. We found that the connectivity pattern of MCs with PNs as well as parvalbumin, vasoactive intestinal peptide, and L1 interneurons exhibit target-specific plasticity and biophysical properties. The specificity of α5-GABA$_A$Rs at MC-PN synapses and the lack or functional expression of this subunit by other cell types define the molecular identity of MC-PN connections and the exclusive involvement of this inhibitory circuits in α5-dependent cognitive tasks.

Introduction

In the neocortex, fast synaptic inhibition underlies important cognitive-relevant activity (Buzsáki, 2010; Isaacson and Scanziani, 2011). Neocortical inhibition is provided by GABAergic interneurons (INs), which are highly heterogeneous and connect with both principal pyramidal neurons (PNs) and other inhibitory cells in a highly stereotyped manner. Some INs, such as parvalbumin (PV)-expressing basket cells, innervate the perisomatic region of cortical PNs, and they thus provide a tight temporal control of PN spiking output and drive cognition-relevant fast network oscillations, especially in the β-γ-frequency range (20-100 Hz) (Bartos et al., 2007; Buzsáki and Wang, 2012).

Conversely, other IN types, such as those expressing the neuropeptide somatostatin (SST), were shown to target dendrites of PNs, thereby controlling dendritic electrogenesis, nonlinear integration, and glutamatergic synaptic input (Wang et al., 2004; Lovett-Barron et al., 2012; Wilson et al., 2012; Schulz et al., 2018). In sensory cortices, SST INs were shown to be involved in lateral inhibition, playing a major role in key sensory computations, such as surround suppression (Kapfer et al., 2007; Silberberg and Markram, 2007; Berger et al., 2009; Adesnik and Scanziani, 2010; Adesnik et al., 2012). Moreover, SST-operated dendritic inhibition was shown to encode fear memory and affective behavior in PFC (Xu et al., 2013; Clem and Cummings, 2020; Scheggia et al., 2020).

SST INs were proposed to be the source of a profuse "blanket" of inhibition because of their dense connectivity with PNs (Fino and Yuste, 2011). However, this view neglects the diversity of SST-positive INs (Riedemann et al., 2016; Gouwens et al., 2020; Zhou et al., 2020; Bugeon et al., 2022), and the fact that they preferentially contact specific PN subclasses (Hilscher et al., 2017) as well as other inhibitory neurons (Pfeffer et al., 2013; Tremblay et al., 2016). In general, SST INs can be classified as Martinotti cells (MCs) and non-MCs, which exhibit differential connectivity patterns as well as specific molecular profiles (Wang et al., 2004; Ma et al., 2006; Tremblay et al., 2016; Yavorska and Wehr, 2016; Paul et al., 2017; Scala et al., 2019; Gouwens et al., 2020; Bugeon et al., 2022). According to the classical description of MCs, these INs exhibit a well-defined axonal morphology, as they project their axons to layer 1, where they extensively inhibit the most distal dendritic tufts of PNs (Wang et al., 2004; Ma et al., 2006; Kapfer et al., 2007; Silberberg and Markram, 2007; Tremblay et al., 2016). Functionally, MCs are efficiently recruited by local PNs with loose-coupled, strongly facilitating synapses (Reyes et al., 1998; Wang et al., 2004; Kapfer et al., 2007; Silberberg and Markram, 2007), and are inhibited by vasoactive intestinal peptide (VIP)-expressing GABAergic INs (Pfeffer et al., 2013; Karnani et al., 2016; Tremblay et al., 2016; Walker et al., 2016). Finally, MCs form synapses with other elements of the cortical circuit, namely, other inhibitory INs (Ma et al., 2006; Pfeffer et al., 2013). However, the actual extent and biophysical properties of these disinhibitory circuits are unknown and/or generalized over SST-expressing MCs and non-MCs (Pfeffer et al., 2013).

Importantly, dendritic inhibition provided by MC-PN synapses is mediated by α5-containing GABA$_A$R (α5-GABA$_A$Rs) (Ali and Thomson, 2008; Zorrilla de San Martin et al., 2020). Similarly, in the hippocampus, dendritic inhibitory synapses from SST-positive INs onto PNs express functional α5-GABA$_A$Rs (Schulz et al., 2018). This prompts the question of whether GABAergic synapses formed by MCs onto other elements of the cortical circuit use this specific subunit of GABA$_A$Rs. Understanding the actual synaptic circuits relying on the α5 subunit has important clinical implications.

Indeed, α5-GABA$_A$Rs were indicated as a prominent target for therapeutic interventions for cognitive dysfunctions in Down syndrome (Braudeau et al., 2011; Schulz et al., 2019; Duchon et al., 2020; Zorrilla de San Martin et al., 2020), depression (Zanos et al., 2017), anesthesia-induced memory impairment (Zurek et al., 2014), and schizophrenia (Duncan et al., 2010; Gill and Grace, 2014). Recent studies described the large diversity of SST-expressing INs (Riedemann et al., 2016; Paul et al., 2017; Gouwens et al., 2020; Zhou et al., 2020; Bugeon et al., 2022) and proposed a number of genetically, morphologically, and functionally defined subclasses highlighting the need for genetic tools to assess the function of these subgroups. Indeed, presently, there are no specific mouse lines that allow the identification and/or manipulation of specific subtypes of SST-expressing INs, including the several subclasses of MCs.

Here we used a transgenic mouse line (*Gad1-GFP*, line X98) (Ma et al., 2006) to assess the connectivity of GFP-expressing MCs (herein defined X98 MCs) in the superficial layers of the mouse barrel cortex. Using this tool, we found that, in addition to the known connectivity with PN distal dendrites, X98 MCs connect extensively also with PV, VIP, and L1 INs, but not with other X98 MCs. Interestingly, GABAergic synapses formed by X98 MCs exhibited clear target specificity of short-term plasticity (STP). Finally, dendritic inhibition using α5-GABA$_A$Rs is a peculiarity of X98 MC-PN synapses, as unitary responses from X98 MCs to other INs exhibited fast (<1 ms) rise time, and they were not modulated by a α5 negative allosteric modulator (NAM).

Together, these results indicate the pharmacological connectivity and biophysical fingerprint used by X98 MCs for inhibitory synapses that they make with PNs and other elements of the cortical circuit.

Materials and Methods

Animals. Experimental procedures followed national and European (2010/63/EU) guidelines and have been approved by the author's institutional review boards and national authorities. All efforts were made to minimize suffering and reduce the number of animals. Mice used in this study were of both sexes. In order to identify GABAergic transmission from different INs, we used several mouse models. To record from PV INs, we initially crossed *Pvalb*-cre mice (The Jackson Laboratory, strain #008069) with a mouse line that expresses a *loxP*-flanked STOP cassette preventing the transcription of a CAG promoter-driven red fluorescent protein variant (tdTomato) (The Jackson Laboratory, strain #007909). Following cre-mediated recombination, the resulting mice exhibit robust tdTomato fluorescence in PV INs. In the experiments illustrated in Figures 2 and 5, we used PValbTomato mouse line (Kaiser et al., 2016) (The Jackson Laboratory, stock #27395), a line that expresses TdTomato fluorescent protein specifically in PV INs. To record from MCs, we used GAD-67-GFP mice, line X98 (Ma et al., 2006) (herein defined as X98; The Jackson Laboratory, stock #006340). To perform simultaneous recordings from X98 MCs and PV INs, we crossed X98 mice with PValb-tdtomato. Furthermore, to record from synaptically connected VIP INs and X98 MCs, we crossed *Vip*-Cre mice (The Jackson Laboratory, strain #010908) with X98 mice (herein defined as VIPcre::X98 mice) and infected newborns with viral vectors carrying the genes of either channelrhodopsin-2 (ChR2) or TdTomato (see below details of different viral infections).

In vitro *slice preparation and electrophysiology.* Coronal slices (300-350 μm thick) from somatosensory cortex were obtained from 18- to 25-d-old mice. This range of ages was chosen to find a compromise between IN maturation (reached before P25 in the somatosensory cortex) (Okaty et al., 2009; Goldberg et al., 2011) and experimental yield. The yield of finding connected pairs of neurons in the cortex decreases starkly with age, notably after postnatal day 25, thus reducing substantially the feasibility of pharmacological treatments during pair recordings in the

different mouse lines used in this study. Animals were deeply anesthetized with isoflurane and decapitated. Brains were quickly removed and immersed in "cutting" solution (4°C) containing the following (in mM): 126 choline, 11 glucose, 26 NaHCO$_3$, 2.5 KCl, 1.25 NaH$_2$PO$_4$, 7 MgSO$_4$, and 0.5 CaCl$_2$ (equilibrated with 95% O$_2$–5% CO$_2$, respectively). Slices were cut with a vibratome (Leica) in the same cutting solution and then incubated in oxygenated aCSF containing the following (in mM): 126 NaCl, 2.5 KCl, 2 CaCl$_2$, 1 MgSO$_4$, 1.25 mM NaH$_2$PO$_4$, 26 mM NaHCO$_3$, and 16 mM glucose (pH 7.4), initially at 34°C for 30 min, and subsequently at room temperature until transfer to the recording chamber. Recordings were obtained at 32°C-34°C. Whole cell voltage-clamp recordings were performed from layer (L)2/3 PNs, MCs, PV, VIP INs, and L1 INs of the primary somatosensory cortex. PNs were visually identified using infrared video microscopy by their large somata and pia-oriented apical dendrites. L1 INs were also visually identified with transmitted light only as they are the only cell type with the soma present in L1. MCs (labeled with GFP, see Fig. 1), VIP INs, and PV INs (labeled with TdTomato) were identified using LED illumination (blue, λ = 470 nm, green λ = 530 nm, OptoLED system, Cairn Research) coupled to epifluorescent optical pathway of the microscope. Single or double voltage-clamp whole cell recordings were made with borosilicate glass capillaries (with a tip resistance of 2-4 MΩ) filled with different intracellular solutions depending on the experiment. For unitary IPSCs (uIPSCs), the intracellular solution contained the following (in mM): 70 K-gluconate, 70 KCl, 10 HEPES, 1 EGTA, 2 MgCl$_2$, 4 Mg-ATP, 0.3 Na-GTP, pH adjusted to 7.2 with KOH, 280-300 mOsm or 145 CsCl, 4.6 MgCl$_2$, 10 HEPES, 1 EGTA, 0.1 CaCl$_2$, 4 Na-ATP, 0.4 Na-GTP, pH adjusted to 7.2 with CsOH, 280-300 mOsm. To confirm the GABAergic nature of uIPSCs, gabazine (10 μm) was added to the aCSF at the end in some experiments. For tonic inhibition experiments, GABA (5 μm) was added to the aCSF. To record unitary EPSCs (uEPSCs) from INs, a low chloride intracellular solution was used and DNQX was omitted in the aCSF superfusate. In these experiments, the intracellular solution had the following composition (in mM): 150 K-gluconate, 4.6 MgCl$_2$, 10 HEPES, 1 EGTA, 0.1 CaCl$_2$, 4 Na-ATP, 0.4 Na-GTP, pH adjusted to 7.2 with KOH, 280-300 mOsm. In voltage-clamp experiments, access resistance was on average <15 MΩ and monitored throughout the experiment. Recordings were discarded from analysis if the resistance changed by >20% over the course of the experiment. Unclamped action currents in presynaptic neurons were elicited in voltage-clamp mode by brief (1 ms) somatic depolarizing steps (from −70 to 0 mV). This resulted in unitary synaptic transmission in simultaneously recorded postsynaptic neurons. A train of 5 presynaptic action currents at 50 Hz was applied to infer STP of synaptic responses. The paired-pulse ratio was obtained as the peak amplitude of the second uEPSC divided by that of the first. In order to isolate GABA$_A$-receptor-mediated currents, DNQX (10 μm) was present in the superfusate of all experiments, unless otherwise indicated.

Signals were amplified, using a Multiclamp 700B patch-clamp amplifier (Molecular Devices), sampled at 20-100 kHz and low-pass filtered at 4 kHz (for voltage-clamp experiments) and 10 kHz (for current-clamp experiments). All drugs were obtained from Tocris Cookson or Sigma. α5IA, (3-(5-methylisoxazol-3-yl)-6-[(1-methyl-1,2,3-triazol-4-yl)methyloxy]-1, 2, 4-triazolo[3, 4-a]phthalazine) also named L-822179 was synthesized by Orga-Link SARL according to Sternfeld et al. (2004) as in Braudeau et al. (2011). The hydrochloride salt was solubilized in DMSO at a concentration of 1 mM and then diluted in the appropriate buffer.

Virus-mediated gene delivery and optogenetics. To study X98 MC-VIP and VIP- X98 MC synapses, we first crossed VIPcre with X98 mice and injected 300 nl of a solution containing adeno-associated viral (AAV) particles into the somatosensory cortex of ice-anesthetized pups (P0-P3) to selectively express TdTomato or ChR2 in VIP INs. Injections were made with a beveled glass pipette 300 μm deep in the somatosensory cortex through intact skin and skull. We then delivered the solution containing the AAVs using a Nanoliter 2000 Injector (WPI). The pipette was left in place for an additional 30 s, before being retracted. The AAVs expressed floxed ChR2 or TdTomato (AAV9.EF1.dflox.hChR2(H134R)-mCherry.WPRE.hGH; Addgene #20297 and pAAV-FLEX-tdTomato; Addgene #28306, respectively) purchased from the Penn Vector Core (University of Pennsylvania). At the end of the procedure, pups were returned to their mother. ChR2 activation was obtained by brief (0.5-

2 ms) LED light pulses on cortical slices (λ = 470 nm). Experiments were performed using a 60× water immersion lens. Light-evoked responses were recorded in L 2/3 MCs and were completely abolished by gabazine (not shown).

Data analysis. Experiments on firing dynamics, tonic currents, and unitary paired recordings were analyzed with Clampfit (Molecular Devices), Origin (OriginLab), and custom-made scripts in MATLAB (The MathWorks). Spontaneous synaptic events were detected using custom written software (Wdetecta, courtesy J. R. Huguenard, Stanford University; https://hlab.stanford.edu/wdetecta.php) based on an algorithm that calculates the derivative of the current trace to find events that cross a certain defined threshold (Ulrich and Huguenard, 1996). Amplitude and rise times of the events were then binned and sorted, using other custom written routines (courtesy J. R. Huguenard, Stanford University).

The peak-to-baseline decay phase of uIPSCs was fitted by the following double exponential function:

$$F(\text{t}) = A_{fast}e^{\frac{-t}{\tau_{fast}}} + A_{slow}e^{\frac{-t}{\tau_{slow}}} \tag{1}$$

where A_{fast} and A_{slow} are the fast and slow amplitude components, and τ_{fast} and τ_{slow} are the fast and slow decay time constants, respectively. The weighted decay time constant ($\tau_{d,w}$) was calculated using the following equation:

$$\tau_{\text{d,w}} = \frac{\left[(A_{fast} \cdot \tau_{fast}) + (A_{slow} \cdot \tau_{slow})\right]}{A_{fast} + A_{slow}} \tag{2}$$

The adaptation index was calculated as the last/first interspike interval ratio following a train of spikes induced by injection of a depolarizing step of current. Passive properties as well as synaptic currents were analyzed with Clampfit and custom-made scripts in MATLAB (The MathWorks). Both unitary and light-induced IPSCs were averaged across at least 20 sweeps for each condition examined. Results are presented as mean ± SEM unless otherwise stated.

Morphologic reconstruction. To reconstruct and quantify anatomic features of different cortical neurons, biocytin (Sigma; catalog #B4261) was included in the intracellular solution at a high concentration (10 mg/ml), which required extensive sonication. To avoid excessive degradation of fragile molecules such as ATP, sonication was performed in an ice bath. The intracellular solution was then filtered twice to prevent the presence of undissolved lumps of biocytin in the patch pipette. Recordings lasted for at least 30 min. We used a high concentration of biocytin to allow efficient filling of axons from recorded INs, as demonstrated previously (Jiang et al., 2015; Scala et al., 2019). This biocytin concentration did not alter the health of the recorded neuron, the incidence of obtaining high-resistance (>1 GΩ) seals, or the stability of whole cell recordings. During that time, access resistance was continuously monitored throughout the experiment. At the end of recordings, the patch pipette was removed carefully to obtain an outside-out patch to reseal the cell properly. The slice was then left in the recording chamber for a further 5-10 min to allow biocytin diffusion. Slices were then fixed with 4% PFA in PBS (Sigma) for at least 48 h. Following fixation, slices were incubated with the avidin-biotin complex (Vector Labs) and a high concentration of detergent (Triton X-100, 5%) for at least 2 d before staining with DAB (Abcam). Cells were then reconstructed, and cortical layers delimited using Neurolucida (MBF Bioscience). Neuronal reconstructions were aligned to a mouse atlas from the Allen Institute. By using Neurolucida Explorer, we analyzed the length of axons and dendrites of MCs in L2/3 and L1 of somatosensory cortex. Data were exported and analyzed in OriginPro 2016 (OriginLab).

Immunofluorescence, confocal imaging, and quantitative imaging analysis. Eighteen- to 25-d-old X98 and VIPcre:X98 mice were anesthetized with ketamine/xylazine (8 μl/g mouse of a 100 mg/ml ketamine and 13 mg/ml xylazine mixture) and transcardially perfused with 1× PBS solution containing heparin (5 IU/ml) followed by 4% (PFA) fixative solution in 1× PBS. Next, brains were dissected and postfixed overnight at 4°C with the same fixative solution. The following day, brains
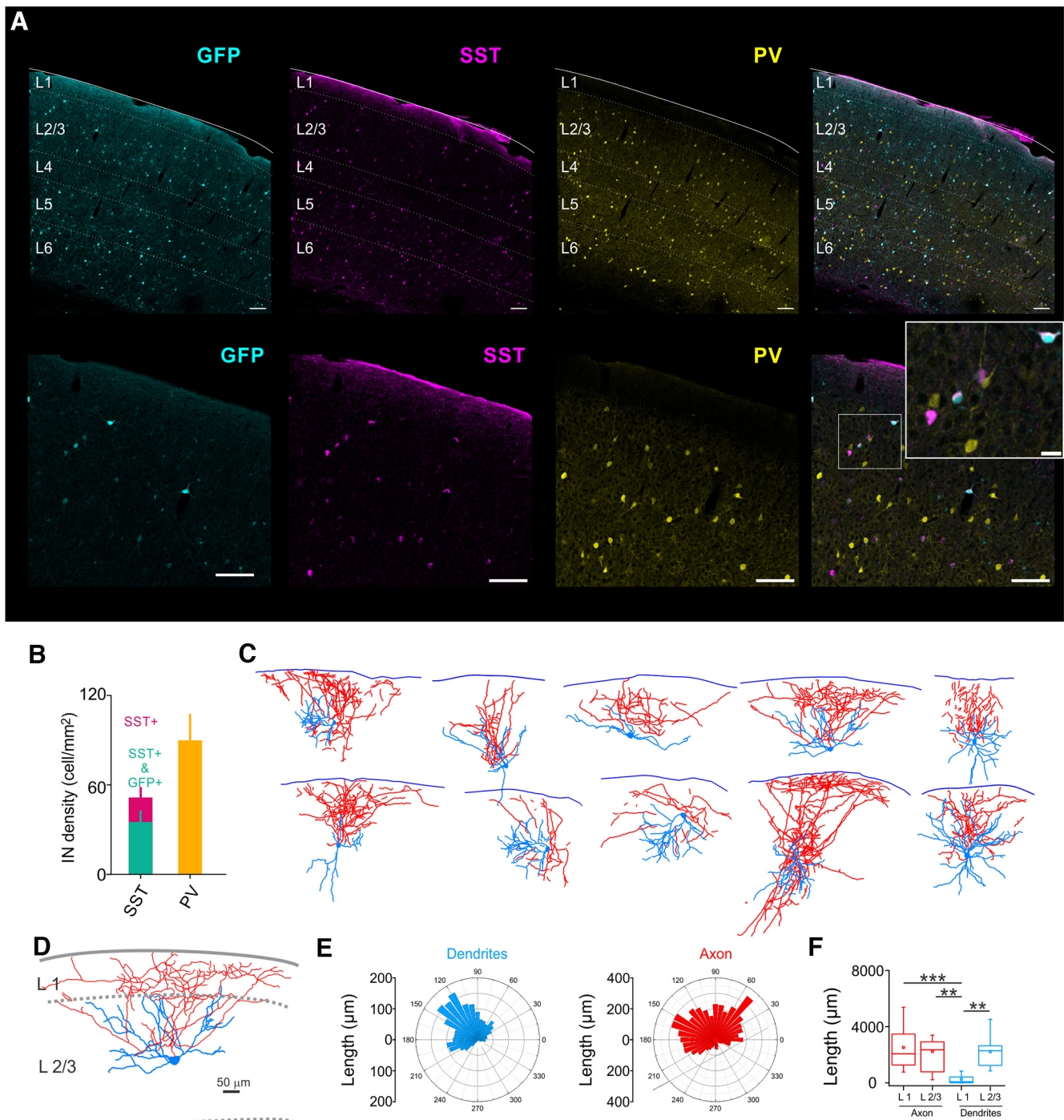
Figure 1. GFP-positive neurons in X98 mice are SST-expressing MCs. *A*, Top panels, Low-magnification confocal micrograph of a triple immune-staining against SST (magenta), PV (yellow), and GFP (cyan) in X98 coronal somatosensory slices. Bottom panels, Detail of L2/3 expression of the same markers shown in *A*. Right, Inset, High-magnification examples of PV-positive, SST-only, and both SST- and GFP-positive cells. *B*, Quantification of cells expressing PV, SST, or SST and GFP in L2/3. *C*, Morphological reconstructions of all GFP-positive neurons filled with biocytin. *D*, Detail of an X98 MC axonal and dendritic interlayer distribution. Blue represents dendrites. Red represents axons. *E*, Axonal (red) and dendritic (blue) polar plots of the cell in *D*. *F*, Population data of axon (red) and dendrite (blue) lengths distribution in L1 and L2/3 ($n = 10$). Scale bars: 100 µm; inset, 10 µm. **$p < 0.01$. ***$p < 0.001$.

were placed overnight in a 30% sucrose solution in $1\times$ PBS for cryoprotection and then frozen in isopentane at a temperature $<-50°C$. Brains were cut into 50-µm-thick coronal sections using a freezing microtome (HM450, Thermo Fisher Scientific) and kept in a 0.4% sodium azide solution at 4°C until immunostaining. For immunostaining for GFP, SST, and PV (see Fig. 1A), free-floating brain sections were permeabilized with a 0.3% Triton X-100 and 10% normal goat serum blocking solution in $1\times$ PBS for 2 h at room temperature. Brain sections were then incubated overnight at 4°C in a 0.003% Triton X-100 and 10% normal goat serum

solution containing the primary antibodies anti-GFP guinea pig (1:1000; Synaptic Systems, 132005), anti-SST mouse (1:1000; Biotechnology, sc-55565), and anti-PV rabbit (1:1000; SWant, PV-28). Brains sections were then washed 3 times for 10 min in $1\times$ PBS and incubated for 3 h at room temperature in a 0.003% Triton X-100 and 10% normal goat serum solution containing the secondary antibodies goat anti-guinea pig (1:500; Invitrogen, A-11073), goat anti-mouse (1:500; Invitrogen, A-21052), and goat anti-rabbit (1:500; Invitrogen, A-31556), conjugated to AlexaFluor-488, -633, and -405, respectively. Brains sections were then washed 3 times

for 10 min in $1\times$ PBS and coverslipped with mounting medium (Fluoromount, Sigma Aldrich, F4680). Before proceeding with immunostaining experiments wherein presynaptic and/or postsynaptic markers (i.e., gephyrin and VGAT) were used (see Fig. 3), free-floating brain sections were subjected to an antigen retrieval procedure using a citrate-based buffer. Briefly, brain sections were washed twice for 10 min in $1\times$ PBS, transferred to a 0.01 M sodium citrate solution, pH 6, and then heated to and maintained at 95°C in water bath for 5 min. Brain sections were washed 3 times for 10 min in $1\times$ PBS and then subjected to the above described permeabilization and immunostaining procedures, using different combinations of antibodies as follows: primary antibodies anti-GFP guinea pig (1:1000; Synaptic Systems, 132005), anti-PV rabbit (1:1000; SWant, PV-28), or anti-PV mouse (1:1000; Sigma Aldrich, P3088) or anti-DsRed mouse (1:500; Takara Bio Clontech, 632392) or anti-DsRed rabbit (1:500; Takara Bio Clontech, 632496) or anti-NeuN mouse (1:500; Merck, MAB377), and anti-gephyrin mouse (1:1000; Synaptic System, 147011) or anti-VGAT rabbit (1:500; Synaptic System, 131002); and secondary antibodies goat anti-guinea pig (1:500; Invitrogen, A-11073) conjugated to AlexaFluor-488, goat anti-mouse (1:500; Invitrogen, A-21052), or anti-rabbit (1:500; Invitrogen, A-21071) conjugated to AlexaFluor-633, and goat anti-mouse (1:500; Invitrogen, A-31553) or anti-rabbit (1:500; Invitrogen, A-31556) conjugated to AlexaFluor-405. The samples were analyzed and images were acquired under a Leica TCS SP8 laser scanning confocal microscope using 405, 488, and 633 nm laser excitation lines in the sequential mode. For the quantification of GFP-, SST-, and PV-positive cells, multiple digital images were captured using a $20\times$ oil-immersion objective lens by a tile scan of the primary somatosensory cortex, which were then combined into a single composite image. The numbers of cells expressing GFP, SST, or PV, as well as double-positive cells for GFP and SST, were manually counted using Cell Counter plugin in ImageJ 1.52a (National Institutes of Health). For the quantification of vGAT-positive terminals (in apposition to GFP-positive axons/puncta) onto somas immunolabeled with antibody against PV, TdTomato, or NeuN, z-stack digital images of 3-5 FOVs in L1 and L2/3 were captured using a $63\times$ oil-immersion objective lens and a zoom factor of $2.5\times$. PV-, TdTomato-, or NeuN-labeled somas were randomly selected for visual quantification of juxtaposed $VGAT^+$ and GFP^+ puncta. Images were deconvolved using Huygens Essential software (Scientific Volume Imaging), and orthogonal projections were obtained by the Fiji version of ImageJ 1.52a (National Institutes of Health).

Statistical analysis. All statistical analyses were performed in Origin (OriginLab). Normality of the data was systematically assessed (Shapiro–Wilk normality test). Normal distributions were statistically compared using paired t test or two-sample t test. When data distributions were not normal or n was small, nonparametric tests were performed (Mann–Whitney, Wilcoxon Signed Ranks Test). Two-way ANOVA tests were followed by Bonferroni's multiple comparison *post hoc*.

Results

The X98 mouse line is a reliable tool to study L2/3 MCs

Despite being broadly classified as dendrite-targeting INs, SST-expressing cells exhibit significant electrophysiological, anatomic, connectivity, and molecular heterogeneity (Ma et al., 2006; Paul et al., 2017; Naka et al., 2019; Gouwens et al., 2020; Bugeon et al., 2022). In order to specifically study the connectivity of L2/3 MCs, we searched for a suitable mouse line. X98 are transgenic mice carrying the gene coding for GFP under control of the *Gad1* promoter. GFP is expressed predominantly in cortical layers (L) 5B and 6, and, to a lesser extent, in L2/3 (Ma et al., 2006). However, although GFP-expressing neurons are present in L2/3, these had not been previously analyzed. Therefore, we first set out to confirm that GFP-expressing neurons in L2/3 belong to the SST-positive IN subtype, broadly defined as the MC.

We performed immunofluorescence staining on microtome-cut coronal somatosensory slices of 18-25-d-old X98 mice (Fig. 1A) and showed that 100% of GFP-expressing neurons also expressed SST, while $32.1 \pm 3.4\%$ of SST-positive and 100% PV-positive INs did not express GFP ($n = 10$ mice; 467 and 807 SST and PV INs, respectively, Fig. 1A,B). Consistent with the previous description of this mouse line (Ma et al., 2006), we also observed a population of GFP-positive non-neuronal cells presenting small soma area (<40 µm^2). These non-neuronal cells were exclusively detectable after immunostaining against GFP (Fig. 1A) but were undetectable during electrophysiological recordings in brain slices.

In another series of experiments, several GFP-expressing neurons were filled with biocytin during whole cell recordings and their morphology was traced to assess somato-dendritic and axonal morphology. Axons of L2/3 GFP-expressing neurons were systematically oriented toward superficial layers and consistently reached L1 where they were profusely branched (Fig. 1C, red tracing; $p = 4.4E^{-4}$, one-way ANOVA followed by Bonferroni *post hoc* test, $F = 7.4716$, $n = 10$ reconstructed GFP-positive neurons). Conversely, GFP-expressing neurons dendrites were mostly located in L2/3 without reaching L1 (Fig. 1C–E, blue tracing).

We then measured the excitability and passive properties of GFP-expressing neurons ($n = 22$) and compared their firing pattern with that of PV INs ($n = 14$), the most abundant and perhaps best characterized GABAergic neuronal subtype (Fig. 2A, B). As previously described, the majority of the GFP-positive cells in X98 mice displayed a characteristic sag in response to hyperpolarizing current injection and a highly adapting firing behavior when depolarizing currents triggered repetitive spiking (Fig. 2B). Conversely, PV INs displayed fast-spiking, non-adapting pattern in response to depolarizing currents (adaptation index: 2.27 ± 0.17 and 1.07 ± 0.04 for GFP-expressing and PV INs, respectively; $p = 1.1E^{-5}$, Mann–Whitney U test; Fig. 2C–E), more hyperpolarized resting membrane potential (V_m: -66 ± 1 and -71 ± 1 mV for GFP-expressing and PV INs, respectively; $p = 0.0017$, unpaired t test) and lower input resistance (R_i: 189 ± 11 and 92 ± 10 MΩ for GFP-expressing and PV INs, respectively; $p = 8.1E^{-6}$, Mann–Whitney U test; Fig. 2B).

We then assessed the biophysical and pharmacological traits of synaptic transmission that distinguish X98 MCs from other INs. We analyzed unitary glutamatergic, excitatory and GABAergic, inhibitory currents (uEPSCs and uIPSCs, respectively) onto and from X98 MCs in X98 MC-PN connected pairs. One hallmark of MC connectivity is the strongly facilitating glutamatergic synaptic responses evoked on PN action potentials (APs) (Wang et al., 2004; Kapfer et al., 2007; Silberberg and Markram, 2007). Accordingly, we found that unitary excitatory inputs from PNs to X98 MCs were invariably facilitating while uEPSCs onto PV INs were depressing (paired-pulse ratio: 1.8 ± 0.2 for GFP-expressing neurons and 0.4 ± 0.1 for PV INs; $p = 1.8E^{-6}$, Mann–Whitney U test; Fig. 1E). Finally, we analyzed the kinetics of uIPSCs elicited by X98 MCs and PV cells in L2/3 PNs. We found that uIPSCs evoked from X98 MCs had significantly slower rise times compared with PV INs (rise time: 1.89 ± 0.25 ms for GFP-expressing neurons and 0.57 ± 0.02 for PV INs; $p = 2.2E^{-5}$, unpaired t test; Fig. 1F), consistent with characteristic MC-mediated dendritic uIPSCs.

Together, these results indicate that GFP-expressing neurons in L2/3 of the somatosensory cortex of X98 mice exhibit morpho-functional features of L2/3 MCs (Wang et al., 2004; Gouwens et al., 2020). GFP-positive neurons in X98 mice (X98 MCs) can be readily distinguished from the most abundant GABAergic PV INs.
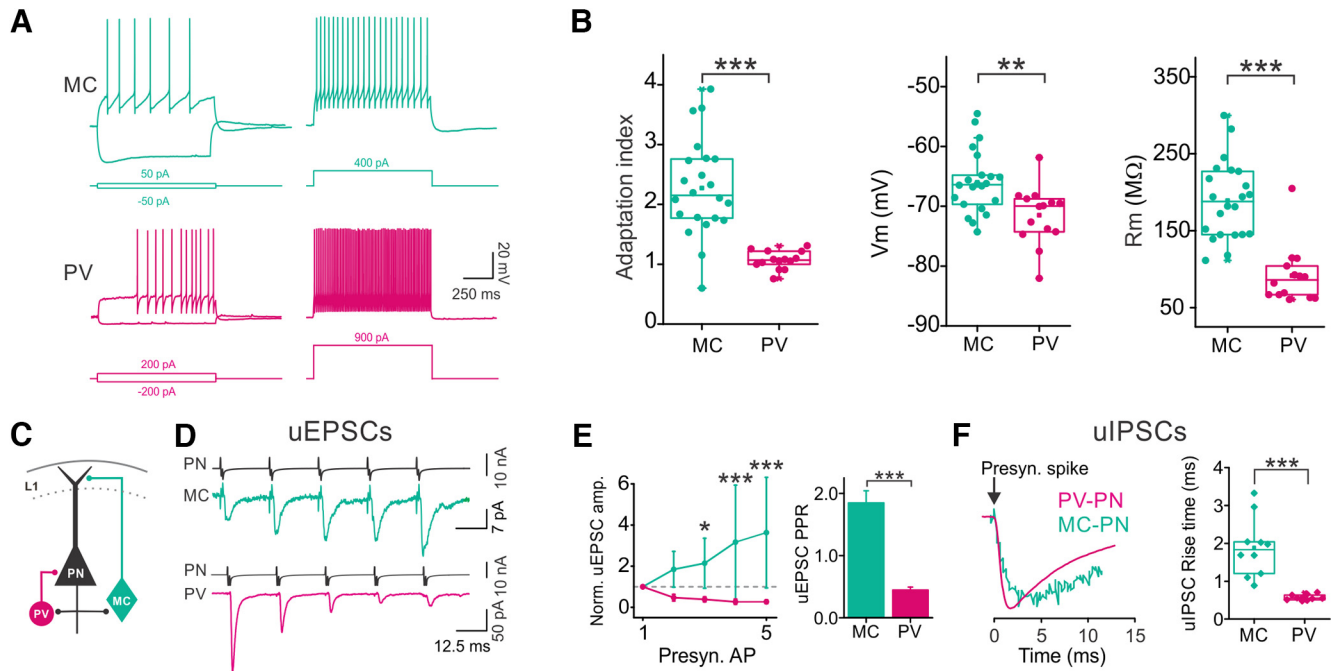
Figure 2. X98 GFP-positive neurons display distinct electrophysiological characteristics of MCs. ***A***, Representative current-clamp recordings from a GFP-expressing IN (green) and a PV cell (red) in X98 mice. X98 GFP cells display a characteristic sag in response to hyperpolarizing current injection and a highly adapting firing behavior. Conversely, PV cells show fast-spiking patterns in response to depolarizing current injections. ***B***, Summary graphs of resting membrane potential (left), membrane resistance (middle), and adaptation index (right) in PV INs ($n = 14$) and MCs ($n = 22$). ***C***, Schematic of mutually connected MC-PN and PV-PN pairs. ***D***, Representative averaged voltage-clamp trace of uEPSCs evoked by 5 APs at 50 Hz in a PN, and recorded in a GFP-positive cell (top, green) and in a PV cell (bottom, magenta) from an X98 mouse. ***E***, Left, Pooled normalized amplitudes of uEPSC evoked with a 50 Hz, 5 AP train. Right, Population plot of paired-pulse ratio of X98 GFP ($n = 20$, green) and PV-INs ($n = 11$, red). ***F***, Left, Overlapped representative uIPSCs elicited by MCs (green) and PV-INs (red) and recorded from PNs. Right, Population plot of the uIPSC mean rise time from MC to PN (green) and PV to PN (red) synapses. *$p < 0.05$. **$p < 0.01$. ***$p < 0.001$.

X98 MCs display target-specific synaptic properties

In addition to PNs, SST INs were shown to contact other inhibitory neurons of the cortical microcircuits, including VIP, PV, and L1 INs (Ma et al., 2006; Pfeffer et al., 2013; Tremblay et al., 2016; Cao et al., 2020). However, it remains unknown whether this is true for X98 MCs and whether these connections exhibit the biophysical and pharmacological properties observed at the inhibitory synapses between X98 MCs and PNs. In order to address this question, we first explored the presence of synaptic markers of inhibitory synaptic contacts from X98 MCs onto other elements of the cortical microcircuit. We found that L2/3 GFP-positive axonal varicosities were juxtaposed to gephyrin-positive puncta located in PV- and VIP-positive somas (Fig. 3A, D) and coexpressed vGAT (Fig. 3B,E), suggesting axo-somatic synaptic contacts of X98-MCs onto PV and VIP INs. Axon terminals coexpressing GFP and vGAT were also juxtaposed to gephyrin-positive puncta around the somas of L1 INs (Fig. 3G, H). Conversely, PV and vGAT labeling onto L2/3 PNs showed characteristic basket structures devoid of GFP-positive axon terminals from X98 MCs (Fig. 3J,K, white asterisk). In order to quantify the incidence of X98 MCs axo-somatic synaptic contacts onto the different neuronal types, we counted the number of GFP- and vGAT-positive puncta juxtaposed to the somas of L2/3 PV-positive, L2/3 VIP-positive, L2/3 NeuN-positive, putative PNs, and L1 NeuN-positive cells. We found that X98 MCs make, on average, 0.94 ± 0.18 synaptic contacts onto PV INs ($n = 47$ cells, 4 mice), 2.04 ± 0.35 onto VIP INs ($n = 28$ cells, 4 mice), 2.03 ± 0.35 onto L1 INs ($n = 34$ cells, 3 mice), and 0.29 ± 0.08 onto L2/3 NeuN-positive cells ($n = 42$ cells, 3 mice; Fig. 3C, F,I,L). Together, these results suggest that X98 MCs make direct, axo-somatic synaptic contacts onto PV, VIP, and L1 INs but not onto PNs.

We then studied the functional characteristics of the synaptic contacts formed by X98 MCs with other cortical INs. We performed dual-patch recordings in brain slices and evoked uIPSCs from specific synapses formed by X98 MCs. To measure and compare evoked uIPSCs from pairs between MCs and other INs, we used brain slices containing differently labeled IN subtypes. For X98 MC-PV synapses, we crossed X98 mice with *Pvalb*-tdTomato mice. For MC-L1 synapses, we used X98 mice and L1 INs were identified by their localization in L1. Finally, to record uIPSCs from MC-VIP cell pairs, we crossed VIPcre with X98 mice. Mouse pups (P1-P3) were then subjected to intracerebral injections of flexed AAV particles coding for the red fluorescent protein tdTomato. We could thus obtain mice, in which MCs and VIP cells were simultaneously labeled with GFP and tdTomato, respectively.

GABAergic synapses formed by MCs to PNs were slow due, at least in part, to their distal dendritic location and consequent electrotonic filtering (Rall, 1967). To further explore whether synaptic contacts made by X98 MCs onto other circuit elements followed a similar pattern, we compared amplitudes and kinetics of uIPSCs elicited by X98 MCs onto PNs, PV-, L1- and VIP-INs (Fig. 4A–F). Rise times of X98 MC-PN uIPSCs were significantly slower than those recorded from X98 MC-PV, X98 MC-L1, and X98 MC-VIP-IN pairs (1.89 ± 0.25; 0.73 ± 0.10; 0.63 ± 0.13; 0.80 ± 0.15 ms, respectively; $p = 1.5\mathrm{E}^{-4}$, one-way ANOVA; $n = 10$, 7, 5, and 6, respectively; Fig. 4F). Rise times of uIPSCs recorded from connected pairs between X98 MCs and PV, VIP and L1 INs were not significantly different (one-way ANOVA followed by Bonferroni *post hoc* test; Fig. 4E). Amplitudes of evoked uIPSCs were also variable between and within connected pairs (Fig. 4F). uIPSC amplitudes were consistently larger in X98 MC-IN than in X98 MC-PN synapses (uIPSC

amplitudes: 10 ± 1; 36 ± 4; 72 ± 32; 172 ± 70 pA; X98 MC-PN, -PV, L1 and VIP INs, respectively; $p = 6.36E^{-4}$; Kruskal Wallis followed by Mann–Whitney with Bonferroni's correction; $n = 10$, 7, 5, and 6 synapses, respectively; Fig. 4E).

We found significant connectivity rates between X98 MCs and PV INs (13 connected of 85 recorded pairs), between X98 MCs and L1 INs (11 connected of 80 recorded pairs), and between X98 MCs and VIP INs (9 connected of 45 recorded pairs; Fig. 4G). Yet, the connectivity rate between X98 MCs and these IN types was much lower than functional connections with PNs (30 connected of 57 recorded pairs; Fig. 4G). Conversely, we did not find functional synaptic transmission between X98 MCs (0 of 10, connected/recorded pairs; Fig. 4G).
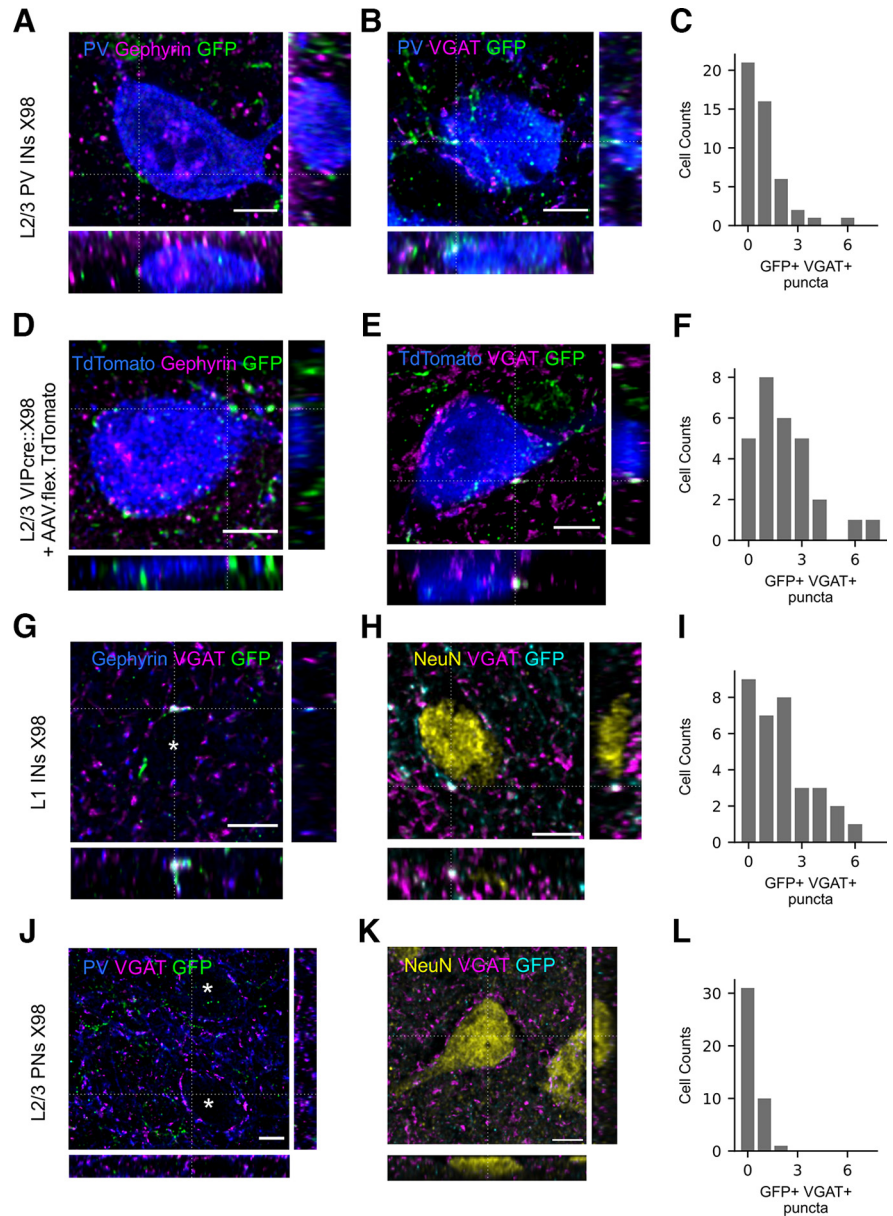
Together, these results indicate that L2/3 X98 MCs preferentially contact PNs, to a lesser, albeit non-negligible, extent PV, VIP, and L1 INs, and avoid connecting between themselves. X98 MC-dendrite targeting is specific for connections with PNs.

We then analyzed STP at all unitary connections made by X98 MCs with different postsynaptic targets (Fig. 5A,B), in response to trains of 5 APs at 50 Hz. We found that STP profiles depended on the postsynaptic target. Indeed, normalized amplitudes of uIPSCs at X98 MC-PN and X98 X98 MC-L1 IN pairs were strongly depressing. In contrast, X98 MC-PV uIPSCs did not vary during the stimulus train, and X98 MC-VIP synapse exhibited a significant facilitating profile (Fig. 5A–C). Compared with X98 MC-PN connections, STP at X98 MC-L1 IN synapses was not significantly different. However, STP of X98 MC-PV and X98 MC-VIP IN synapses was significantly different from X98 MC-PN connections (repeated-measures, two-way ANOVA followed by Bonferroni *post hoc* test; $F = 24.1516$, $p = 7.34E^{-5}$, $n = 5$, 7, 5, and 7 synapses for X98 MC-VIP, -PV, -L1, and -PN, respectively; Fig. 3B,C).

Although we observed variability within the different synaptic contact types analyzed, together these results suggest that STP at X98 MC-synapses exhibits target specificity reflecting synapse-specific presynaptic and postsynaptic mechanisms.


Figure 3. X98 MCs make axo-somatic contacts onto L2/3 PV-, VIP-, and L1-INs but not PNs. *A*, Confocal micrographs of X98 L2/3 somatosensory cortex slices immunostained against PV (blue), GFP (green), and gephyrin (magenta) or (*B*) PV (blue), GFP (green), and vGAT (magenta). *C*, Number of X98 MC contacts onto L2/3 PV INs. Distribution of the number of GFP- and vGAT-positive puncta per PV-positive soma. *D*, Confocal micrographs of L2/3 somatosensory cortex slices immunostained against TdTomato (pseudocolored in blue), GFP (green), and gephyrin (magenta) or (*E*) TdTomato (blue), GFP (green), and vGAT (magenta) in VIPcre::X98 mice infected with AAV.flex.tdTomato. *F*, Number of X98 MC contacts onto L2/3 VIP INs. Distribution of the number of GFP- and vGAT-positive puncta juxtaposed to the soma of VIP INs. *G*, L1 X98 somatosensory cortex slice immunostained against GFP (green), VGAT (magenta), and gephyrin (blue) or (*H*) GFP (cyan), VGAT (magenta), and NeuN (yellow). *I*, Distribution of the number of GFP- and vGAT-positive puncta juxtaposed to the soma of L1 INs. Histogram represents the distribution of the number of GFP- and vGAT-positive puncta per L1 NeuN-positive soma. *J*, L2/3 X98 somatosensory cortex slice immunostained against GFP (green), vGAT (magenta), and PV (blue) or (*K*) GFP (cyan), VGAT (magenta), and NeuN (yellow). *L*, Number of GFP- and vGAT-positive puncta juxtaposed to the soma of L2/3 NeuN-positive, putative PNs. Distribution of the number of GFP- and vGAT-positive puncta per soma of L2/3 NeuN-positive, putative PN. *G*, *J*, *Immunolabeling gap produced by unlabeled somas. Scale bars, 5 μm.

α5-GABA$_A$Rs define X98 MC-PN synapses in L2/3 of mouse somatosensory cortex

Synaptic transmission between MCs and PNs was shown to be mediated by GABA$_A$Rs containing the α5 subunit in the rat somatosensory cortex (Ali and Thomson, 2008); in the mouse PFC (Zorrilla de San Martin et al., 2020) and in the SST-expressing, oriens-lacunosum moleculare (OL-M) INs to

PN synapse (Schulz et al., 2018). Furthermore, in the rat somatosensory cortex, PV-IN-mediated PN perisomatic inhibition is sensitive to zolpidem (100 nM), a positive allosteric modulator, which at this concentration, is known to specifically bind to the benzodiazepine site of α1-containing and, less efficiently, α2- and α3-containing GABA$_A$ receptors (Korpi et al., 2002; Möhler, 2002; Bacci et al., 2003). In order to validate these results in the
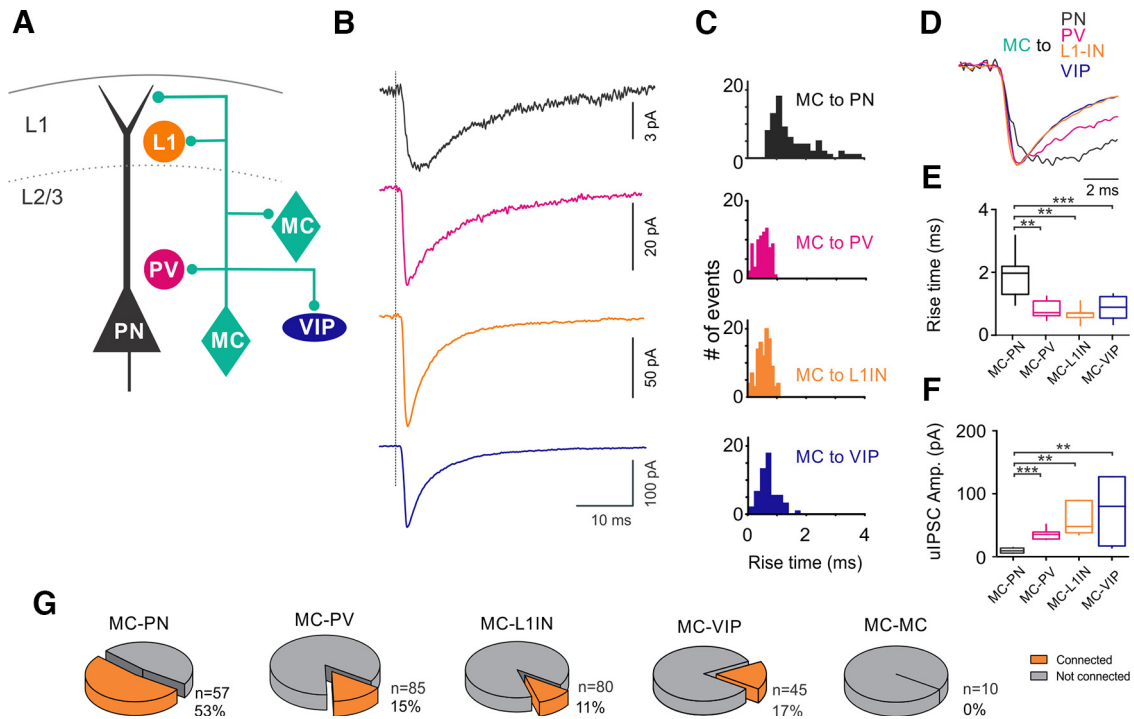
Figure 4. Diversity of X98 MC connectivity onto different neuronal types in the L2/3 of somatosensory cortex. ***A***, Schematic representation of the tested inhibitory connections involving MCs. ***B***, Representative voltage-clamp uIPSC average traces from MC to PN (black), PV (magenta), L1 (orange), and VIP (blue) INs. Gray dotted line indicates the time of the peak of presynaptic APs. ***C***, Representative distributions of uIPSC rise time recorded from individual MC-PN (black), MC-PV (magenta), MC-L1 (orange), and MC-VIP (blue) connections. ***D***, uIPSC (same as in ***C***) normalized to the peak. ***E***, Population plot of the mean uIPSC amplitudes from individual MC-PN, MC-PV, MC-L1, and MC-VIP recorded connections. ***F***, Population plot of the mean uIPSC rise times from individual MC-PN, MC-PV, MC-L1, and MC-VIP recorded connections. ***G***, Pie charts represent the connectivity rates of MC-MC, MC-L1, MC-VIP, MC-PV, and MC-PN synapses. **p < 0.01. ***p < 0.001.
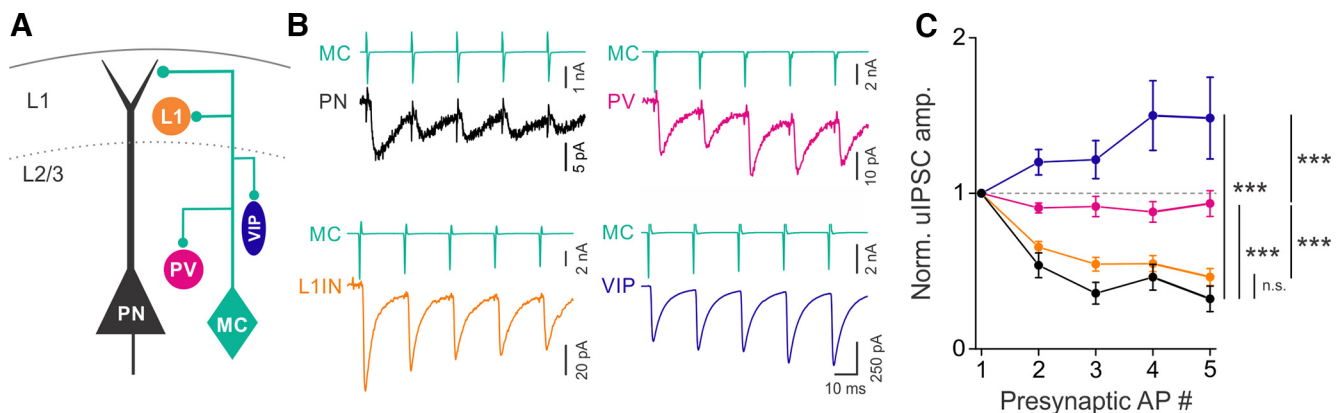

Figure 5. Plasticity of X98 MC-mediated synaptic inhibition in L2/3 of somatosensory cortex. ***A***, Schematic representation of the tested inhibitory circuits involving MCs. ***B***, Representative voltage-clamp averaged traces of uIPSCs from MCs onto PNs (black), PV (magenta), L1 (orange), and VIP (blue) INs. ***C***, Normalized uIPSC amplitudes elicited by MCs onto different elements of the L2/3 inhibitory circuit. Inhibition of MCs onto PN (black) and L1 INs (orange) is strongly depressing, whereas MC connections onto VIP (blue) INs are facilitating. The strength of MC-PV synapses was overall unchanged during repetitive presynaptic stimulations. ***p < 0.001.

mouse somatosensory cortex, we tested the effects of α5IA, a NAM specific for α5-GABA$_A$Rs (Dawson et al., 2006), and zolpidem on both X98 MC-mediated PN dendritic inhibition and PV-IN-mediated PN perisomatic inhibition (Fig. 6A). PV-PN uIPSC weighted decay time constant ($\tau_{d,w}$) was significantly increased by zolpidem (control: 9.0 ± 1.3 ms; zolpidem: 11.2 ± 0.7 ms, $n = 6$ pairs, $p = 0.014$, paired *t* test; Fig. 6B, left). In contrast, PV-PN uIPSC amplitude was unaffected by α5IA (control: 63 ± 22 pA; α5IA: 65 ± 20 pA, $n = 6$ pairs, $p = 0.7294$, paired *t* test; Fig. 6B, right). The amplitude of uIPSCs elicited from X98 MCs was highly sensitive to α5IA (control: 177 ± 44 pA;

α5IA: 104 ± 23 pA, $n = 11$ pairs; $p = 0.003$, Wilcoxon signed-ranks test; Fig. 6C, right), and zolpidem did not affect the weighted decay time constant of the X98 MC-PN uIPSCs (control: 8.2 ± 1.2 ms; zolpidem: 9.1 ± 0.9, $n = 6$ pairs, $p = 0.173$, paired *t* test; Fig. 6C, left). α5IA is a partial NAM displaying $\sim$40% efficacy, thus not providing a complete blockade of α5-GABA$_A$Rs (Dawson et al., 2006). Accordingly, after incubation with α5IA, the remaining X98 MC-PN uIPSC amplitude was near 60% (65.7 ± 5.4%; Fig. 6C). This suggests that unitary synaptic responses from X98 MCs to PNs are fully mediated by α5-GABA$_A$Rs.
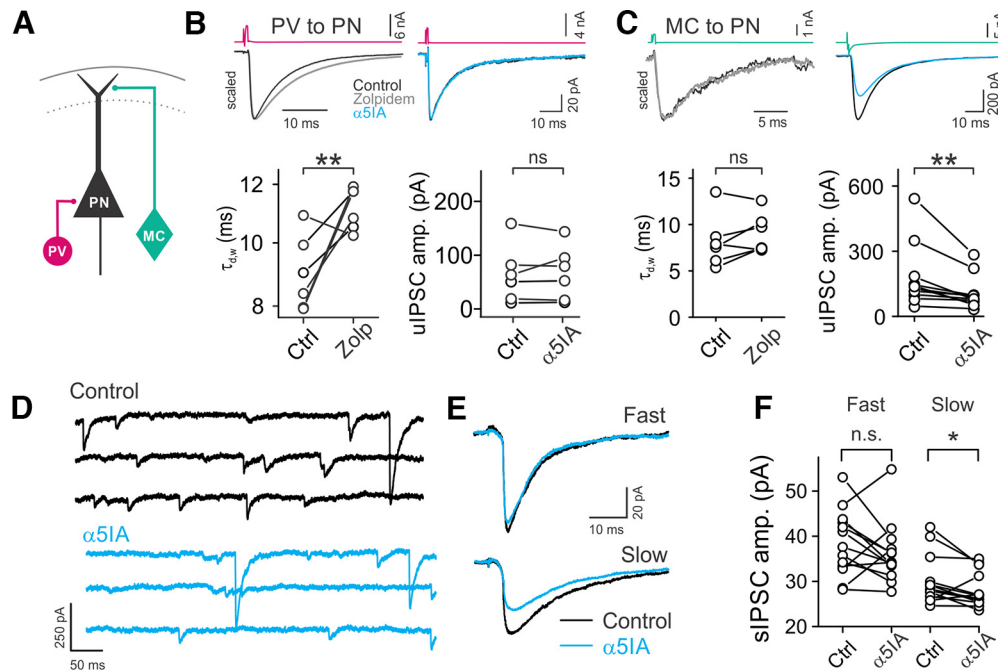
Figure 6. α5-GABA$_A$Rs mediate synaptic inhibition selectively from X98 MCs. **A**, Schematic representation of paired recordings between an MC or PV and a PN. **B**, Top left, Representative average uIPSC traces elicited by a PV onto a PN in the absence (black) and presence (gray) of zolpidem. Traces are scaled to highlight zolpidem effect on uIPSC decay time. Bottom left, Population data of zolpidem effect on the weighted decay time constant ($\tau_{d,w}$, left). Top right, Representative average uIPSC traces elicited by a PV cell onto a PN in the absence (black) and presence (blue) of α5IA. Bottom right, Population data of α5IA effect on uIPSC amplitudes in PV-PN pairs. **C**, Same as in **B**, but for MC-PN pairs. **D**, Representative voltage-clamp traces of sIPSCs recorded from a PN before (control, black) and after 15 minutes incubation with 100 nM α5IA (blue). MC-PN synapse uIPSCs recorded with nonphysiological, Cs-based, high chloride, internal solution (see Materials and Methods). **E**, Representative averaged traces of fast (top) and slow (bottom) events recorded from the PN in **D**. Only amplitudes of slow events are affected by α5IA (bottom, blue trace). **F**, Population plot of individual cells, fast and slow sIPSC median amplitudes measured in control and after incubation with α5IA. *$p < 0.05$. **$p < 0.01$.

α5-GABA$_A$Rs have been hypothesized to be extrasynaptic, mainly mediating tonic inhibition (Caraiscos et al., 2004). However, there is growing evidence that α5-GABA$_A$Rs are also involved in dendritic inhibition at specific synapses made by MCs in the cortex and by oriens-lacunosum moleculare INs in the hippocampus (Ali and Thomson, 2008; Schulz et al., 2018; Zorrilla de San Martin et al., 2020). It is possible that sensitivity of uIPSCs to α5IA could be partially or fully because of activation of extrasynaptic GABA$_A$Rs because of GABA spillover, induced by AP-evoked synaptic transmission. To further study the role of synaptic α5-GABA$_A$Rs, we measured spontaneous IPSCs (sIPSCs) recorded from PNs (Fig. 6D–F). Because quantal, AP-independent synaptic events make up a large fraction of sIPSCs, these are less likely shaped by activation of extrasynaptic receptors. To separate putative dendritic and perisomatic events, we sorted sIPSCs into two groups based on their rise times (Fig. 6D–F). We considered the events with rise times >1.8 ms as "slow," whereas those with rise times <1.8 ms were defined as "fast," based on the average rise time obtained at connected X98 MC-PN pairs (Fig. 1F). The amplitudes of slow sIPSCs were significantly reduced after 10 min incubation with 100 nM α5IA (control: 31 ± 2 pA, α5IA: 28 ± 1 pA, $n = 11$ cells, $p = 0.03$, Wilcoxon signed-ranks test; Fig. 6E). Conversely, the same concentration of α5IA did not affect fast sIPSC amplitude (control: 38 ± 2 pA, α5IA: 36 ± 2 pA; $n = 11$ cells, $p = 0.3636$, Wilcoxon signed-ranks test; Fig. 6F). This result indicates that fast, perisomatic events are generated by other INs types, not using α5-GABA$_A$Rs.

Together, these results indicate that synapses formed by dendrite-targeting X98 MCs onto PNs, specifically express α5-GABA$_A$Rs, whereas PV-PN synapses express α1-GABA$_A$Rs.

X98 MCs inhibit PNs, but not other INs, through α5-GABA$_A$Rs

In the previous sections, we showed that X98 MCs make synaptic contacts exhibiting target-specific biophysical and physiological properties. We also showed that, among the inhibitory inputs received by PNs, those originating from X98 MCs are distinguished by their sensitivity to α5IA. We therefore tested whether postsynaptic expression of α5-GABA$_A$Rs is a trait shared by all synaptic contacts made by X98 MCs or it is specific for synaptic contacts that X98 MCs form on PN dendrites. To address this question, we measured unitary GABAergic synaptic transmission between X98 MCs and other INs and tested their sensitivity to α5IA. We found that uIPSC amplitudes elicited by X98 MCs and recorded in PV INs (control: 31 ± 4 pA, α5IA: 35 ± 6 pA, $n = 11$ pairs, $p = 0.3757$, paired t test), L1 INs (control: 83 ± 32 pA, α5IA: 102 ± 29 pA, $n = 5$ pairs, $p = 0.3757$, paired t test), and VIP INs (control: 178 ± 100 pA, α5IA: 118 ± 52 pA, $n = 4$ pairs, $p = 0.7432$, Wilcoxon signed ranks test) were not sensitive to α5IA (Fig. 7B,C).

In the hippocampus, SST-positive, oriens-lacunosum moleculare INs receive α5-mediated inhibition from VIP INs (Magnin et al., 2019). Since VIP-MC synapses represent an important disinhibitory circuit in the cortex as well, we tested whether α5-GABA$_A$Rs mediate inhibitory inputs from VIP INs also in the mouse somatosensory cortex. To address this question, we crossed VIP-cre with X98 mice (VIP-cre::X98 mice). Since dual whole cell recordings produced a very low yield (3 connected of 45 recorded pairs), we expressed the light-sensitive opsin ChR2 via injection of flexed-ChR2 AAV particles in the barrel cortex of 1- to 3-d-old VIP-cre::X98 pups. We activated VIP INs and recorded light-evoked IPSCs in X98 MCs. We found that
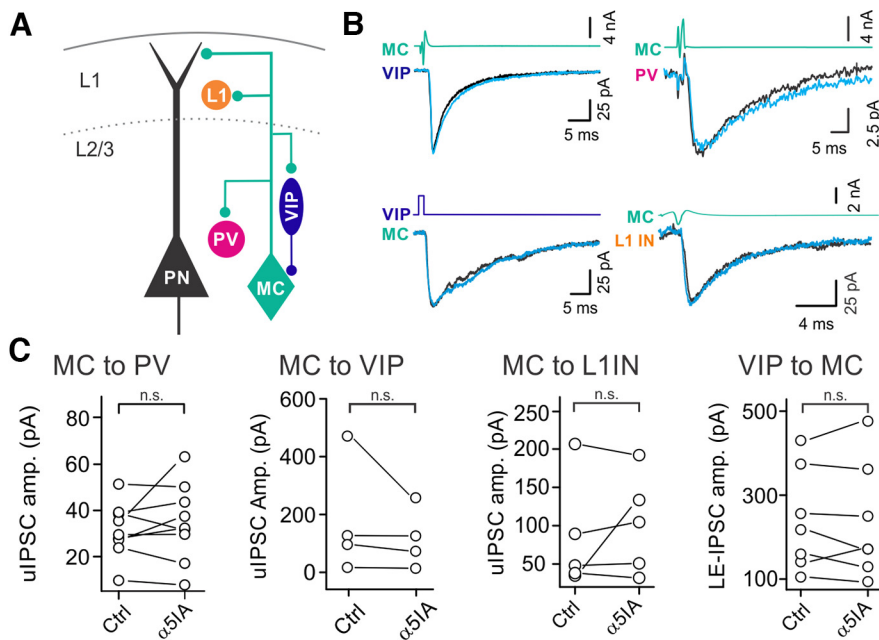
Figure 7. Inhibitory synaptic transmission involving MCs and other INs does not rely on α5-GABA$_A$Rs. **A**, Schematic representation of the tested inhibitory circuits involving MCs. **B**, Representative averaged voltage-clamp traces of uIPSCs from MCs onto different element of the circuit and from VIP to MC before (black) and after (blue) application of α5IA. **C**, Population data of uIPSC amplitude before (Ctrl) and 15 minutes after α5IA application.

inhibitory responses originating from VIP cells were not sensitive to α5IA (control: 170 ± 46 pA, α5IA: 166 ± 52 pA, $n = 7$, $p = 0.7432$, Wilcoxon signed ranks test; Fig. 7B).

Overall, these results indicate that GABAergic inhibition involving X98 MCs uses α5-GABA$_A$Rs exclusively at synapses formed with PN distal dendrites and not for other X98 MC-targets within cortical circuits. Thus, the characteristic slow kinetics of uIPSCs, the distal dendritic targeting, and the synaptic expression of α5-GABA$_A$Rs represent unique molecular and cellular signatures of X98 MC-PN synapses.

Tonic inhibition is mediated by α5-GABA$_A$Rs in PN, but not in X98 MC nor PV-IN

α5-GABA$_A$Rs have been largely associated to tonic inhibition because of extrasynaptic immunoreactivity in cell culture (Loebrich et al., 2006; Serwanski et al., 2006), hippocampus and cortex (Serwanski et al., 2006), and amygdala (Botta et al., 2015) and the lack of tonic inhibitory current in hippocampal PNs of α5 KO mice (Caraiscos et al., 2004).

Thus, we preincubated slices with aCSF or aCSF + 100 nM α5IA during at least 10 min and then quantified the difference in holding current amplitude (ΔI_{hold}) before and after bath application of 1 μM gabazine (Fig. 8). Preincubation with 100 nM α5IA significantly reduced GABAergic ΔI_{hold} in PNs compared with slices preincubated in aCSF only (aCSF: 51 ± 1 pA, $n = 16$; α5IA: 29 ± 7 pA, $n = 23$, $p = 0.0244$, unpaired t test; Fig. 8A,B). Conversely, incubation with α5IA failed to produce any significant change in tonic current recorded from X98 MCs (aCSF: 16 ± 5 pA, $n = 9$; α5IA: 23 ± 6 pA, $n = 14$, $p = 0.3330$, unpaired t test; Fig. 8C,D) nor PV INs (aCSF: 33 ± 10 pA, $n = 9$; α5IA: 24 ± 5 pA, $n = 14$, $p = 0.6591$, unpaired t test; Fig. 8E,F), showing that tonic inhibition is mediated by α5-GABA$_A$Rs exclusively in PNs.

Together, these results indicate that α5-GABA$_A$Rs are selectively expressed by PNs and they mediate both tonic and dendritic phasic synaptic inhibition.

Discussion

In this study, we explored physiological aspects of different inhibitory synaptic connections made by a subset of SST-positive INs in the L2/3 of the mouse somatosensory cortex, the X98 MCs. We show that inhibitory synapses made by X98 MCs display biophysical, morphologic, and pharmacological properties that are specific in distinct postsynaptic partners. We found that the most extensively contacted cells are PNs. However, also PV, VIP, and L1 inhibitory INs also receive significant inhibition from X98 MCs. Notably, we showed that the X98 MC-PN synapse is distinguished by two unique features: slow kinetics and expression of the α5-GABA$_A$R. Finally, we showed that α5-GABA$_A$Rs contribute to tonic inhibition of PNs but not of other INs, confirming the specific involvement of this receptor in PN dendritic inhibition.

SST-cre mouse lines are widely used to study the functional role of SST-expressing INs by manipulating and recording their activity, using cre-driven expression of light-sensitive opsins or genetically encoded Ca^{2+} sensors (Taniguchi et al., 2011). Despite its extensive use, the SST-cre mouse line affects all INs expressing SST. Yet, SST-positive neurons encompass a highly heterogeneous group of inhibitory neurons that display diverse molecular profile, morphology, spiking patterns, and connectivity (Halabisky et al., 2006; Ma et al., 2006; McGarry et al., 2010; Riedemann et al., 2016; Naka et al., 2019; Gouwens et al., 2020; Zhou et al., 2020; Bugeon et al., 2022). Here we provide evidence that GFP-expressing neurons in the somatosensory cortex of young (P18-25) X98 mice account for 68% of SST-expressing INs and exhibit morpho-functional properties of L2/3 MCs (Wang et al., 2004; Kapfer et al., 2007; Silberberg and Markram, 2007; Tremblay et al., 2016; Gouwens et al., 2020). Previous estimates indicate that the subpopulation of GFP-expressing neurons from X98 adult mice represents a specific subset of GABAergic INs, accounting for 16% (all layers) or 13% (L2/3) of all SST neurons (Ma et al., 2006). This discrepancy could be because of developmental differences between the range of ages used in this study and that of the original quantification (2-3 months after birth) (Ma et al., 2006), or simply to differences in the sample size used in this and the original study. Since this mouse line is based on the GAD promoter and a random insertion into the mouse genome (Ma et al., 2006), we cannot rule out the possibility of other subtypes of MCs that do not express GFP and thus were not included in our experiments. However, our results indicate that GFP-positive neurons encompass a large majority of SST-expressing INs, which belong to the broad class of SST-expressing MCs. Determining whether GFP-positive neurons in X98 mice comprehensively capture a specific MC subclass will require RNAseq analysis from GFP-expressing neurons (Gouwens et al., 2020; Bugeon et al., 2022).

Although X98 MCs extensively inhibit PNs via α5-GABA$_A$Rs, they also contact other elements of the cortical microcircuits; and, in addition, they are targeted by VIP-
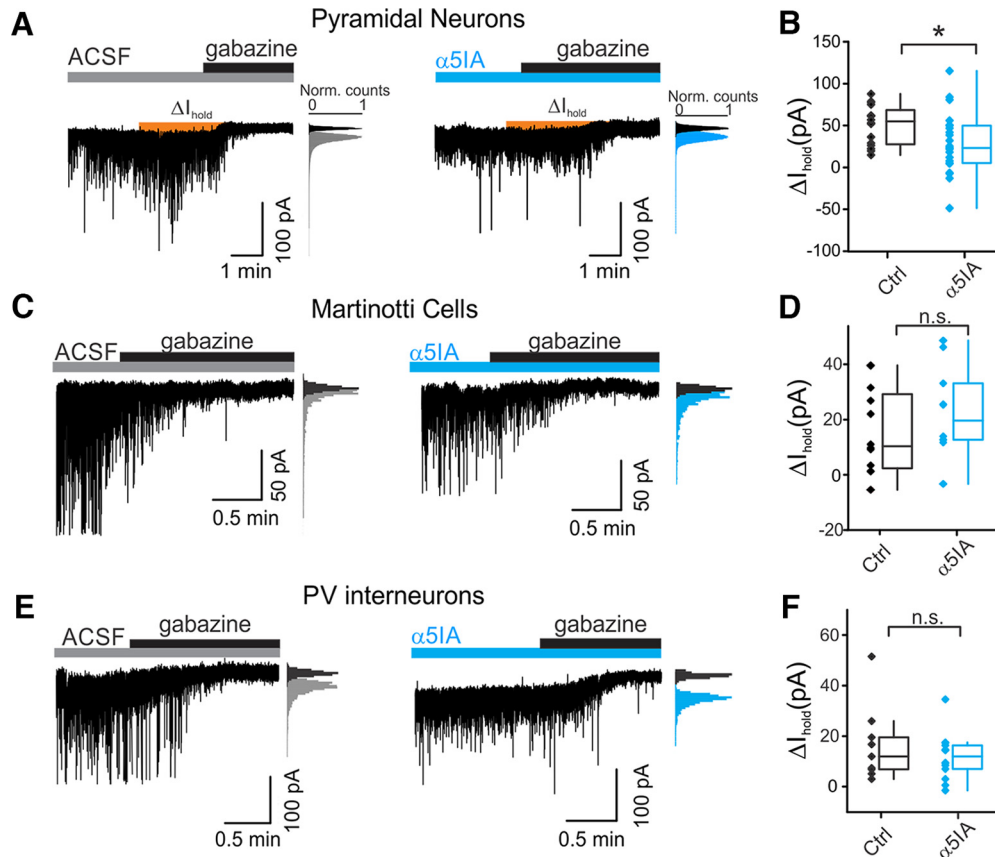
Figure 8. α5GABA$_A$Rs only contribute to tonic inhibition in L2/3 PN of mouse somatosensory cortex. ***A***, Whole-cell voltage-clamp recordings from L2/3 PNs preincubated with either vehicle (aCSF, left) or α5IA (right). DNQX (10 μM) and GABA (5 μM) were continuously present in both conditions. Orange areas (ΔI$_{hold}$) represent tonic inhibition measured after gabazine onset. Insets, All-points histograms of the current trace obtained in the absence (gray and blue histograms) and presence of gabazine (black histograms). Gaussian fits were used to determine the noise half-width. ***C-E***, Same as in ***A***, but for MCs and PV-INs, correspondingly. ***B***, ***D***, ***F***, Population graphs of holding-current shifts after gabazine application (ΔI$_{hold}$). *$p < 0.05$.

expressing INs (Pfeffer et al., 2013; Kepecs and Fishell, 2014; Tremblay et al., 2016; Walker et al., 2016). We found that X98 MCs contact PV-, VIP-, and L1-INs at a reduced connectivity rate compared with X98 MC-PN connections. Moreover, GABAergic synapses from X98 MCs onto other INs and those inhibiting X98 MCs from VIP-INs do not use α5-GABA$_A$Rs.

MCs were hypothesized to provide a nonspecific "blanket" of inhibition to PNs (Fino and Yuste, 2011; Fino et al., 2013; Karnani et al., 2016). Accordingly, we found a relatively high connectivity rate between X98 MCs and L2/3 PNs, consistent with the prominent X98 MC axonal plexus innervating L1. In addition to PN dendrites, despite at lower rate, X98 MCs contact also L1-INs, which exert slow feedforward inhibition on PN dendrites during the encoding of context-rich, top-down information from higher-order thalamus and cortices (Letzkus et al., 2011; Abs et al., 2018). X98 MC-L1 IN connectivity was relatively low. However, we could have underestimated X98 MC-L1 IN connectivity, as we did not discriminate different L1 IN subclasses. Indeed, SST INs have been reported to privilege NDNF-positive INs of L1 (Abs et al., 2018).

Importantly, dendritic inhibition seems to be a specific feature of X98 MC-PN connections, as uIPSC rise times measured on other X98 MC targets (INs) had fast (<1 ms) kinetics similar to the known PV-PN perisomatic responses. In agreement with this view, we failed to find evidence of direct contact between X98 MC axons on the perisomatic region of PNs. Conversely, we found X98 MC VGAT-positive boutons juxtaposed to the

gephyrin-positive puncta onto the perisomatic region of PV, VIP, and L1 INs. This is consistent with the fast, nonfiltered, IPSCs observed in somatic whole cell recordings and in line with a previous report showing that inhibitory contacts onto PV INs are preferentially located in the proximal dendrites and soma, while excitatory inputs are located in distal dendrites (Kameda et al., 2012).

Use-dependent short-term facilitation or depression of synaptic responses has been traditionally linked to specific synaptic mechanisms identifying diverse cell types with specific presynaptic and postsynaptic biophysical properties, such as low or high release probability, respectively (Jackman and Regehr, 2017). Importantly, frequency-dependent bidirectional STP is a powerful synaptic tool to provide distinct cell types with a specific strategy to transfer information about presynaptic spike trains. We found that GABAergic synapses from X98 MCs exhibit target cell-specific facilitation and depression. Target cell-specific STP and release probability, originating from the same cell type, was described at glutamatergic synapses from PNs recruiting different IN subtypes in the neocortex and hippocampus (Reyes et al., 1998). Our finding indicates that single-axon, target-specific bidirectional STP occurs also at GABAergic synapses. Intriguingly, synapses made in L1 (with either PN distal dendrites or sparse INs) are depressing, whereas inhibitory connection that the same cells make onto their targets in L2/3 (PV and VIP cells) is either unvarying or strongly facilitating. It will be interesting to reveal the molecular and synaptic mechanisms underlying the target specificity of GABAergic synapses originating from the same X98

MC onto different elements of the cortical circuit. Interestingly, STP of unitary inhibitory-to-inhibitory synapses from PV and SST cells was shown to be determined by the identity of the presynaptic IN (Ma et al., 2012). Target cell type-dependent variability in presynaptic properties increases the computational power of neuronal networks. It will be therefore fundamental to understand the functional role of such a target-specific regulation of inhibitory synaptic efficacy.

X98 MCs exhibit differential inhibitory strategies depending on the postsynaptic cell type: they modulate input onto PNs and they likely control, at least in part, the output activity of other INs. Therefore, inhibitory circuits formed by X98 MCs seem to exhibit a more complex architecture and function than previously hypothesized as provider of a mere blanket of inhibition (Fino and Yuste, 2011).

In addition to the strong preference for distal apical dendrites, X98 MCs display another PN-specific synaptic feature, as they use α5-GABA$_A$Rs for synaptic dendritic inhibition. Indeed, GABAergic synapses from X98 MCs to other INs are perisomatic and do not use α5-GABA$_A$Rs. Indeed, lack of α5IA effects on tonic inhibition on PV and X98 MCs suggests that these major IN subtypes do not express this GABA$_A$R α subunit. This is in line with gene expression results in different cortical neuron subtypes, indicating PNs as majorly expressing α5-GABA$_A$Rs (Hu et al., 2019). Transcriptomics analysis of different GABA$_A$R subunits in specific cortical IN subclasses indicates relative low expression of *Gabra5* in all IN subclasses compared with *Gabra1* and *Gabra2* (Winterer et al., 2019). Yet, we cannot exclude that other IN subtypes might use α5-GABA$_A$Rs at their inhibitory synapses with PNs and other INs. Interestingly, it has been recently reported that hippocampal oriens-lacunosum moleculare INs also express α5-GABA$_A$Rs at synapses originating at VIP INs (Magnin et al., 2019). Yet, we did not find evidence of α5IA effect on VIP-IN-evoked IPSCs in X98 MCs of the barrel cortex, suggesting that cortical MCs differ from their hippocampal counterparts. The α5 subunit is much more strongly expressed in the hippocampus than in the neocortex (Lingford-Hughes et al., 2002). Therefore, it will be interesting to reveal whether α5 has different circuit specificity and/or plays a different role in these two areas. Likewise, it remains to be tested whether α5-GABA$_A$Rs are also expressed by other subtypes of inhibitory neurons. Our results on L1-INs suggest that X98 MCs do not use α5-GABA$_A$Rs at these synapses. However, L1 is populated by a heterogeneous IN population (Schuman et al., 2019); and since we did not use specific mouse lines to target distinct cell types, our data may have been collected from a relatively heterogeneous IN group. Overall, our results are consistent with a previous report indicating that synapses from SST$^+$ INs to other nonspecified INs are insensitive to α5-IA (Cao et al., 2020).

In addition to dendritic filtering, X98 MC-PN synaptic responses might be slow because of the specific properties of the α5-subunit itself, which is exclusively expressed at this synapse. The slow kinetics and the rectification of α5-GABA$_A$Rs match the biophysical properties of NMDARs, which govern Ca^{2+} signaling and dendritic computation in PNs (Branco and Häusser, 2010; Tran-Van-Minh et al., 2015; Schulz et al., 2018). Dendritic patch would be necessary to test this hypothesis, although the high series resistance typical of dendritic patch recordings might prevent an accurate analysis of fast currents.

α5-GABA$_A$Rs have been proposed to mediate tonic inhibition because of their sensitivity to nanomolar concentrations of GABA, their nondesensitizing properties, and the lack of

evidence supporting its implication in synaptic transmission (Caraiscos et al., 2004). However, knockdown of radixin, the extrasynaptic scaffolding protein associated to α5-GABA$_A$Rs, did not produce any effect on GABA-evoked current, suggesting that extrasynaptic α5-GABA$_A$Rs might not be functional (Loebrich et al., 2006). Furthermore, the participation of α5-GABA$_A$Rs in phasic synaptic inhibition has been recently demonstrated in different brain structures, namely, the rat somatosensory cortex (Ali and Thomson, 2008), mouse hippocampus (Schulz et al., 2018; Lodge et al., 2021), and mouse PFC (Zorrilla de San Martin et al., 2020). Even for AP-dependent unitary responses between X98 MCs and PNs, it is possible that GABA could spill over to perisynaptic or extrasynaptic GABA$_A$Rs containing α5. If this were the case, we would not have detected significant effects on quantal events, which reflect mostly purely synaptic activation of GABA$_A$Rs. Importantly, we recorded sIPSCs from the soma of L2/3 PNs and found that only slow sIPSCs were sensitive to α5IA, whereas fast perisomatic inhibitory events were unaffected. Our results on sIPSCs corroborate the synaptic localization of α5-GABA$_A$Rs. Indeed, at our extracellular K$^+$ concentrations, sIPSCs are dominated by AP-independent miniature events. The blockade of X98 MC-PN uIPSCs, slow sIPSCs, and tonic inhibition was not total, but it was in all cases maximal, taking into account the actual efficacy ($\sim$40%) of α5IA (Sternfeld et al., 2004; Atack, 2010).

Therefore, the most parsimonious interpretation of our pharmacological experiments is that α5-GABA$_A$Rs are prominently expressed at synaptic sites of dendritic X98 MC-PN connections and are responsible for dendritic inhibition from this specific GABAergic neuron type. Indeed, the α5-mediated tonic currents could be the direct activation by ambient GABA of high-affinity synaptic, and not necessarily extrasynaptic, receptors. However, we cannot exclude that both synaptic and extrasynaptic α5-GABA$_A$Rs receptors exist and dynamically interact (see Hausrat et al., 2015).

The specific expression of the α5 GABA$_A$R subunit in PNs is particularly interesting in light of its involvement in cognitive processes. Mice lacking the *Gabra5* gene, encoding for the α5 subunit of the GABA$_A$R, show enhanced performance in cognitive tasks (Collinson et al., 2002). This evidence, in addition to the high α5-GABA$_A$Rs expression in the mouse PFC and hippocampus (Fritschy and Mohler, 1995), led to propose novel potential pro-cognitive pharmacological strategies in several brain disorders, such as intellectual disability in Down syndrome, memory deficits, and depression (Braudeau et al., 2011; Martínez-Cué et al., 2013; Duchon et al., 2020; Zorrilla de San Martin et al., 2020; Zurek et al., 2014; Zanos et al., 2017). Specific negative modulation of these receptors would facilitate cognition avoiding anxiogenic and pro-convulsive effects of wide-spectrum GABA$_A$Rs antagonists because of the restricted expression of the α5 subunit to this specific inhibitory circuit formed by MCs.

References

Abs E, Poorthuis RB, Apelblat D, Muhammad K, Pardi MB, Enke L, Kushinsky D, Pu DL, Eizinger MF, Conzelmann KK, Spiegel I, Letzkus JJ (2018) Learning-related plasticity in dendrite-targeting layer 1 interneurons. Neuron 100:684–699.e5.

Adesnik H, Scanziani M (2010) Lateral competition for cortical space by layer-specific horizontal circuits. Nature 464:1155–1160.

Adesnik H, Bruns W, Taniguchi H, Huang ZJ, Scanziani M (2012) A neural circuit for spatial summation in visual cortex. Nature 490:226–231.

Ali AB, Thomson AM (2008) Synaptic α5 subunit-containing GABAA receptors mediate IPSPs elicited by dendrite-preferring cells in rat neocortex. Cereb Cortex 18:1260–1271.

Atack JR (2010) Preclinical and clinical pharmacology of the GABAA receptor α5 subtype-selective inverse agonist α5IA. Pharmacol Ther 125:11–26.

Bacci A, Rudolph U, Huguenard JR, Prince DA (2003) Major differences in inhibitory synaptic transmission onto two neocortical interneuron subclasses. J Neurosci 23:9664–9674.

Bartos M, Vida I, Jonas P (2007) Synaptic mechanisms of synchronized gamma oscillations in inhibitory interneuron networks. Nat Rev Neurosci 8:45–56.

Berger TK, Perin R, Silberberg G, Markram H (2009) Frequency-dependent disynaptic inhibition in the pyramidal network: a ubiquitous pathway in the developing rat neocortex. J Physiol 587:5411–5425.

Botta P, Demmou L, Kasugai Y, Markovic M, Xu C, Fadok JP, Lu T, Poe MM, Xu L, Cook JM, Rudolph U, Sah P, Ferraguti F, Lüthi A (2015) Regulating anxiety with extrasynaptic inhibition. Nat Neurosci 18:1493–1500.

Branco T, Häusser M (2010) The single dendritic branch as a fundamental functional unit in the nervous system. Curr Opin Neurobiol 20:494–502.

Braudeau J, Delatour B, Duchon A, Pereira PL, Dauphinot L, de Chaumont F, Olivo-Marin JC, Dodd R, Hérault Y, Potier MC (2011) Specific targeting of the GABA-A receptor α5 subtype by a selective inverse agonist restores cognitive deficits in Down syndrome mice. J Psychopharmacol 25:1030–1042.

Bugeon S, Duffield J, Dipoppa M, Ritoux A, Prankerd I, Nicoloutsopoulos D, Orme D, Shinn M, Peng H, Forrest H, Viduolyte A, Reddy CB, Isogai Y, Carandini M, Harris KD (2022) A transcriptomic axis predicts state modulation of cortical interneurons. Nature 607:330–338.

Buzsáki G (2010) Neural syntax: cell assemblies, synapsembles, and readers. Neuron 68:362–385.

Buzsáki G, Wang XJ (2012) Mechanisms of gamma oscillations. Annu Rev Neurosci 35:203–225.

Cao JW, Guan W, Yu YC, Fu Y (2020) Synaptic transmission from somatostatin-expressing interneurons to excitatory neurons mediated by α5-subunit-containing GABAA receptors in the developing visual cortex. Neuroscience 449:147–156.

Caraiscos VB, Elliott EM, You-Ten KE, Cheng VY, Belelli D, Newell JG, Jackson MF, Lambert JJ, Rosahl TW, Wafford KA, MacDonald JF, Orser BA (2004) Tonic inhibition in mouse hippocampal CA1 pyramidal neurons is mediated by alpha5 subunit-containing gamma-aminobutyric acid type A receptors. Proc Natl Acad Sci USA 101:3662–3667.

Clem RL, Cummings KA (2020) Prefrontal somatostatin interneurons encode fear memory. Nat Neurosci 23:61–74.

Collinson N, Kuenzi FM, Jarolimek W, Maubach KA, Cothliff R, Sur C, Smith A, Otu FM, Howell O, Atack JR, McKernan RM, Seabrook GR, Dawson GR, Whiting PJ, Rosahl TW (2002) Enhanced learning and memory and altered GABAergic synaptic transmission in mice lacking the alpha 5 subunit of the GABAA receptor. J Neurosci 22:5572–5580.

Dawson GR, Maubach KA, Collinson N, Cobain M, Everitt BJ, MacLeod AM, Choudhury HI, McDonald LM, Pillai G, Rycroft W, Smith AJ, Sternfeld F, Tattersall FD, Wafford KA, Reynolds DS, Seabrook GR, Atack JR (2006) An inverse agonist selective for α5 subunit-containing GABA A receptors enhances cognition. J Pharmacol Exp Ther 316:1335–1345.

Duchon A, Gruart A, Albac C, Delatour B, Zorrilla de San Martin J, Delgado-García JM, Hérault Y, Potier MC (2020) Long-lasting correction of in vivo LTP and cognitive deficits of mice modelling Down syndrome with an α5-selective GABAA inverse agonist. Br J Pharmacol 177:1106–1118.

Duncan CE, Webster MJ, Rothmond DA, Bahn S, Elashoff M, Shannon Weickert C (2010) Prefrontal GABAA receptor α-subunit expression in normal postnatal human development and schizophrenia. J Psychiatr Res 44:673–681.

Fino E, Packer AM, Yuste R (2013) The logic of inhibitory connectivity in the neocortex. Neuroscientist 19:228–237.

Fino E, Yuste R (2011) Dense inhibitory connectivity in neocortex. Neuron 69:1188–1203.

Fritschy JM, Mohler H (1995) GABAA receptor heterogeneity in the adult rat brain: differential regional and cellular distribution of seven major subunits. J Comp Neurol 359:154–194.

Gill K, Grace A (2014) The role of α5 GABAA receptor agonists in the treatment of cognitive deficits in schizophrenia. Curr Pharm Des 20:5069–5076.

Goldberg EM, Jeong HY, Kruglikov I, Tremblay R, Lazarenko RM, Rudy B (2011) Rapid developmental maturation of neocortical FS cell intrinsic excitability. Cereb Cortex 21:666–682.

Gouwens NW, et al. (2020) Integrated morphoelectric and transcriptomic classification of cortical GABAergic cells. Cell 183:935–953.e19.

Halabisky B, Shen F, Huguenard JR, Prince DA (2006) Electrophysiological classification of somatostatin-positive interneurons in mouse sensorimotor cortex. J Neurophysiol 96:834–845.

Hausrat TJ, Muhia M, Gerrow K, Thomas P, Hirdes W, Tsukita S, Heisler FF, Herich L, Dubroqua S, Breiden P, Feldon J, Schwarz JR, Yee BK, Smart TG, Triller A, Kneussel M (2015) Radixin regulates synaptic GABAA receptor density and is essential for reversal learning and short-term memory. Nat Commun 6:6872.

Hilscher MM, Leão RN, Edwards SJ, Leão KE, Kullander K, Bacci A (2017) Chrna2-Martinotti cells synchronize layer 5 type A pyramidal cells via rebound excitation. PLoS Biol 15:e2001392.

Hu X, Rocco BR, Fee C, Sibille E (2019) Cell type-specific gene expression of alpha 5 subunit-containing gamma-aminobutyric acid subtype A receptors in human and mouse frontal cortex. Mol Neuropsychiatry 4:204–215.

Isaacson JS, Scanziani M (2011) How inhibition shapes cortical activity. Neuron 72:231–243.

Jackman SL, Regehr WG (2017) The mechanisms and functions of synaptic facilitation. Neuron 94:447–464.

Jiang X, Shen S, Cadwell CR, Berens P, Sinz F, Ecker AS, Patel S, Tolias AS (2015) Principles of connectivity among morphologically defined cell types in adult neocortex. Science 350:139–148.

Kaiser T, Ting JT, Monteiro P, Feng G (2016) Transgenic labeling of parvalbumin-expressing neurons with tdTomato. Neuroscience 321:236–245.

Kameda H, Hioki H, Tanaka YH, Tanaka T, Sohn J, Sonomura T, Furuta T, Fujiyama F, Kaneko T (2012) Parvalbumin-producing cortical interneurons receive inhibitory inputs on proximal portions and cortical excitatory inputs on distal dendrites. Eur J Neurosci 35:838–854.

Kapfer C, Glickfeld LL, Atallah BV, Scanziani M (2007) Supralinear increase of recurrent inhibition during sparse activity in the somatosensory cortex. Nat Neurosci 10:743–753.

Karnani MM, Jackson J, Ayzenshtat I, Sichani XH, Manoocheri K, Kim S, Yuste R (2016) Opening holes in the blanket of inhibition: localized lateral disinhibition by VIP interneurons. J Neurosci 36:3471–3480.

Kepecs A, Fishell G (2014) Interneuron cell types are fit to function. Nature 505:318–326.

Korpi ER, Mihalek RM, Sinkkonen ST, Hauer B, Hevers W, Homanics GE, Sieghart W, Lüddens H (2002) Altered receptor subtypes in the forebrain of GABAA receptor δ subunit-deficient mice: recruitment of γ2 subunits. Neuroscience 109:733–743.

Letzkus JJ, Wolff SB, Meyer EM, Tovote P, Courtin J, Herry C, Lüthi A (2011) A disinhibitory microcircuit for associative fear learning in the auditory cortex. Nature 480:331–335.

Lingford-Hughes A, Hume SP, Feeney A, Hirani E, Osman S, Cunningham VJ, Pike VW, Brooks DJ, Nutt DJ (2002) Imaging the GABA-benzodiazepine receptor subtype containing the alpha5-subunit in vivo with [11C]Ro15 4513 positron emission tomography. J Cereb Blood Flow Metab 22:878–889.

Lodge M, Hernandez MC, Schulz JM, Bischofberger J (2021) Sparsification of AP firing in adult-born hippocampal granule cells via voltage-dependent α5-GABAA receptors. Cell Rep 37:109768.

Loebrich S, Bä Hring R, Katsuno T, Tsukita S, Kneussel M (2006) Activated radixin is essential for GABA A receptor a5 subunit anchoring at the actin cytoskeleton. EMBO J 25:987–999.

Lovett-Barron M, Turi GF, Kaifosh P, Lee PH, Bolze F, Sun XH, Nicoud JF, Zemelman BV, Sternson SM, Losonczy A (2012) Regulation of neuronal input transformations by tunable dendritic inhibition. Nat Neurosci 15:423–430.

Ma Y, Hu H, Agmon A (2012) Short-term plasticity of unitary inhibitory-to-inhibitory synapses depends on the presynaptic interneuron subtype. J Neurosci 32:983–988.

Ma Y, Hu H, Berrebi AS, Mathers PH, Agmon A (2006) Distinct subtypes of somatostatin-containing neocortical interneurons revealed in transgenic mice. J Neurosci 26:5069–5082.

Magnin E, Francavilla R, Amalyan S, Gervais E, David LS, Luo X, Topolnik L (2019) Input-specific synaptic location and function of the $\alpha5$ GABA a receptor subunit in the mouse CA1 hippocampal neurons. J Neurosci 39:788–801.

Martínez-Cué C, Martinez P, Rueda N, Vidal R, Garcia S, Vidal V, Corrales A, Montero JA, Pazos A, Florez J, Gasser R, Thomas AW, Honer M, Knoflach F, Trejo JL, Wettstein JG, Hernandez MC (2013) Reducing GABAA 5 receptor-mediated inhibition rescues functional and neuro-morphological deficits in a mouse model of Down syndrome. J Neurosci 33:3953–3966.

McGarry LM, Packer AM, Fino E, Nikolenko V, Sippy T, Yuste R (2010) Quantitative classification of somatostatin-positive neocortical interneur-ons identifies three interneuron subtypes. Front Neural Circuits 4:12.

Möhler H (2002) Pathophysiological aspects of diversity in neuronal inhibi-tion: a new benzodiazepine pharmacology. Dialogues Clin Neurosci 4:261–269.

Naka A, Veit J, Shababo B, Chance RK, Risso D, Stafford D, Snyder B, Egladyous A, Chu D, Sridharan S, Mossing DP, Paninski L, Ngai J, Adesnik H (2019) Complementary networks of cortical somatostatin interneurons enforce layer specific control. Elife 8:e43696.

Okaty BW, Miller MN, Sugino K, Hempel CM, Nelson SB (2009) Transcriptional and electrophysiological maturation of neocortical fast-spiking GABAergic interneurons. J Neurosci 29:7040–7052.

Paul A, Crow M, Raudales R, He M, Gillis J, Huang ZJ (2017) Transcriptional architecture of synaptic communication delineates GABAergic neuron iden-tity. Cell 171:522–539.e20.

Pfeffer CK, Xue M, He M, Huang ZJ, Scanziani M (2013) Inhibition of inhi-bition in visual cortex: the logic of connections between molecularly dis-tinct interneurons. Nat Neurosci 16:1068–1076.

Rall W (1967) Distinguishing theoretical synaptic potentials computed for different soma-dendritic distributions of synaptic input. J Neurophysiol 30:1138–1168.

Reyes A, Lujan R, Rozov A, Burnashev N, Somogyi P, Sakmann B (1998) Target cell-specific facilitation and depression in neocortical circuits. Nat Neurosci 1:279–285.

Riedemann T, Schmitz C, Sutor B (2016) Immunocytochemical heterogene-ity of somatostatin-expressing GABAergic interneurons in layers II and III of the mouse cingulate cortex: a combined immunofluorescence/design-based stereologic study. J Comp Neurol 524:2281–2299.

Scala F, Kobak D, Shan S, Bernaerts Y, Laturnus S, Cadwell CR, Hartmanis L, Froudarakis E, Castro JR, Tan ZH, Papadopoulos S, Patel SS, Sandberg R, Berens P, Jiang X, Tolias AS (2019) Layer 4 of mouse neocortex differs in cell types and circuit organization between sensory areas. Nat Commun 10:12.

Scheggia D, Managò F, Maltese F, Bruni S, Nigro M, Dautan D, Latuske P, Contarini G, Gomez-Gonzalo M, Requie LM, Ferretti V, Castellani G, Mauro D, Bonavia A, Carmignoto G, Yizhar O, Papaleo F (2020) Somatostatin interneurons in the prefrontal cortex control affective state discrimination in mice. Nat Neurosci 23:47–60.

Schulz JM, Knoflach F, Hernandez MC, Bischofberger J (2018) Dendrite-tar-geting interneurons control synaptic NMDA-receptor activation via non-linear $\alpha5$-GABAA receptors. Nat Commun 9:3576.

Schulz JM, Knoflach F, Hernandez MC, Bischofberger J (2019) Enhanced dendritic inhibition and impaired NMDAR activation in a mouse model of down syndrome. J Neurosci 39:5210–5221.

Schuman B, Machold RP, Hashikawa Y, Fuzik J, Fishell GJ, Rudy B (2019) Four unique interneuron populations reside in neocortical layer 1. J Neurosci 39:125–139.

Serwanski DR, Miralles CP, Christie SB, Mehta AK, Li X, Blas AD (2006) Synaptic and non-synaptic localization of GABA A receptors containing the $\alpha5$ subunit in the rat brain. J Comp Neurol Neurol 499:458–470.

Silberberg G, Markram H (2007) Disynaptic inhibition between neocortical pyramidal cells mediated by Martinotti cells. Neuron 53:735–746.

Sternfeld F, Carling RW, Jelley RA, Ladduwahetty T, Merchant KJ, Moore KW, Reeve AJ, Street LJ, O'Connor D, Sohal B, Atack JR, Cook S, Seabrook G, Wafford K, Tattersall FD, Collinson N, Dawson GR, Castro JL, MacLeod AM (2004) Selective, orally active γ-aminobutyric acidA $\alpha5$ receptor inverse agonists as cognition enhancers. J Med Chem 47:2176–2179.

Taniguchi H, He M, Wu P, Kim S, Paik R, Sugino K, Kvitsiani D, Fu Y, Lu J, Lin Y, Miyoshi G, Shima Y, Fishell G, Nelson SB, Huang ZJ (2011) A resource of Cre driver lines for genetic targeting of GABAergic neurons in cerebral cortex. Neuron 71:995–1013.

Tran-Van-Minh A, Cazé RD, Abrahamsson T, Cathala L, Gutkin BS, DiGregorio DA (2015) Contribution of sublinear and supralinear dendri-tic integration to neuronal computations. Front Cell Neurosci 9:67.

Tremblay R, Lee S, Rudy B (2016) GABAergic interneurons in the neocortex: from cellular properties to circuits. Neuron 91:260–292.

Ulrich D, Huguenard JR (1996) GABA(B) receptor-mediated responses in GABAergic projection neurones of rat nucleus reticularis thalami in vitro. J Physiol 493:845–854.

Walker F, Möck M, Feyerabend M, Guy J, Wagener RJ, Schubert D, Staiger JF, Witte M (2016) Parvalbumin-and vasoactive intestinal polypeptide-expressing neocortical interneurons impose differential inhibition on Martinotti cells. Nat Commun 7:13664.

Wang Y, Toledo-Rodriguez M, Gupta A, Wu C, Silberberg G, Luo J, Markram H (2004) Anatomical, physiological and molecular properties of Martinotti cells in the somatosensory cortex of the juvenile rat. J Physiol 561:65–90.

Wilson NR, Runyan CA, Wang FL, Sur M (2012) Division and subtraction by distinct cortical inhibitory networks in vivo. Nature 488:343–348.

Winterer J, Lukacsovich D, Que L, Sartori AM, Luo W, Földy C (2019) Single cell RNA-Seq characterization of anatomically identified OLM interneur-ons in different transgenic mouse lines. Eur J Neurosci 50:3750–3771.

Xu H, Jeong HY, Tremblay R, Rudy B (2013) Neocortical somatostatin-expressing GABAergic interneurons disinhibit the thalamorecipient layer 4. Neuron 77:155–167.

Yavorska I, Wehr M (2016) Somatostatin-expressing inhibitory interneurons in cortical circuits. Front Neural Circuits 10:76.

Zanos P, Nelson ME, Highland JN, Krimmel SR, Georgiou P, Gould TD, Thompson SM (2017) A negative allosteric modulator for $\alpha5$ subunit-containing GABA receptors exerts a rapid and persistent antidepressant-like action without the side effects of the NMDA receptor antagonist ke-tamine in mice. eNeuro 4:ENEURO.0285-16.2017-301.

Zhou X, Mansori I, Fischer T, Witte M, Staiger JF (2020) Characterizing the morphology of somatostatin-expressing interneurons and their synaptic innervation pattern in the barrel cortex of the GFP-expressing inhibitory neurons mouse. J Comp Neurol 528:244–260.

Zorrilla de San Martin J, Donato C, Peixoto J, Aguirre A, Choudhary V, De Stasi AM, Lourenço J, Potier MC, Bacci A (2020) Alterations of specific cortical GABAergic circuits underlie abnormal network activity in a mouse model of Down syndrome. Elife 9:1–54.

Zurek AA, Yu J, Wang DS, Haffey SC, Bridgwater EM, Penna A, Lecker I, Lei G, Chang T, Salter EW, Orser BA (2014) Sustained increase in $\alpha5$GABAareceptor function impairs memory after anesthesia. J Clin Invest 124:5437–5441.